UPPSALA
UNIVERSITET

Digital Comprehensive Summaries of Uppsala Dissertations from the Faculty of Science and Technology 1135

Electronic Structures and Energy Level Alignment in Mesoscopic Solar Cells

A Hard and Soft X-ray Photoelectron Spectroscopy Study

REBECKA LINDBLAD

ACTA
UNIVERSITATIS
UPSALIENSIS
UPPSALA
2014

ISSN 1651-6214
ISBN 978-91-554-8921-2
urn:nbn:se:uu:diva-221450

Dissertation presented at Uppsala University to be publicly examined in Polhemsalen, Ångströmlaboratoriet, Lägerhyddsvägen 1, Uppsala, Friday, 23 May 2014 at 10:15 for the degree of Doctor of Philosophy. The examination will be conducted in English. Faculty examiner: Prof. Dr. Marcus Bär (Helmholtz-Zentrum Berlin für Materialen und Energie).

Abstract
Lindblad, R. 2014. Electronic Structures and Energy Level Alignment in Mesoscopic Solar Cells. A Hard and Soft X-ray Photoelectron Spectroscopy Study. *Digital Comprehensive Summaries of Uppsala Dissertations from the Faculty of Science and Technology* 1135. 87 pp. Uppsala: Acta Universitatis Upsaliensis. ISBN 978-91-554-8921-2.

Photoelectron spectroscopy is an experimental method to study the electronic structure in matter. In this thesis, a combination of soft and hard X-ray based photoelectron spectroscopy has been used to obtain atomic level understanding of electronic structures and energy level alignments in mesoscopic solar cells. The thesis describes how the method can be varied between being surface and bulk sensitive and how to follow the structure linked to particular elements. The results were discussed with respect to the material function in mesoscopic solar cell configurations.

The heart of a solar cell is the charge separation of photoexcited electrons and holes, and in a mesoscopic solar cell, this occurs at interfaces between different materials. Understanding the energy level alignment between the materials is important for developing the function of the device. In this work, it is shown that photoelectron spectroscopy can be used to experimentally follow the energy level alignment at interfaces such as TiO_2/metal sulfide/polymer, as well as TiO_2/perovskite.

The electronic structures of two perovskite materials, $CH_3NH_3PbI_3$ and $CH_3NH_3PbBr_3$ were characterized by photoelectron spectroscopy and the results were discussed with support from quantum chemical calculations. The outermost levels consisted mainly of lead and halide orbitals and due to a relatively higher cross section for heavier elements, hard X-ray excitation was shown useful to study the position as well as the orbital character of the valence band edge.

Modifications of the energy level positions can be followed by core level shifts. Such studies showed that a commonly used additive in mesoscopic solar cells, Li-TFSI, affected molecular hole conductors in the same way as a p-dopant. A more controlled doping can also be achieved by redox active dopants such as Co(+III) complexes and can be studied quantitatively with photoelectron spectroscopy methods.

Hard X-rays allow studies of hidden interfaces, which were used to follow the oxidation of Ti in stacks of thin films for conducting glass. By the use of soft X-rays, the interface structure and bonding of dye molecules to mesoporous TiO_2 or ZnO could be studied in detail. A combination of the two methods can be used to obtain a depth profiling of the sample.

Keywords: Photoelectron spectroscopy, HAXPES, PES, XPS, electronic structure, energy level alignment, mesoscopic solar cell, hole conductor, perovskite, dye-sensitized, semiconductor-sensitized, TiO2, ZnO, spiro-OMeTAD, P3HT, DEH, metal sulfide, Li-TFSI, Co(+III) complex

Rebecka Lindblad, Department of Physics and Astronomy, Molecular and condensed matter physics, Box 516, Uppsala University, SE-751 20 Uppsala, Sweden.

ISSN 1651-6214
ISBN 978-91-554-8921-2
urn:nbn:se:uu:diva-221450 (http://urn.kb.se/resolve?urn=urn:nbn:se:uu:diva-221450)

"An experiment is a question which science poses to Nature
and a measurement is the recording of Nature's answer."
Max Planck

"A well balanced anode running at 10000 rpm can
hardly be heard in a normal laboratory environment."
Ulrik Gelius

Till min familj, stor som liten

List of papers

This thesis is based on the following papers, which are referred to in the text by their Roman numerals.

I. **Preventing dye aggregation on ZnO by adding water in the dye-sensitization process**
Rebecka Schölin, Maria Quintana, Erik M. J. Johansson, Maria Hahlin, Tannia Marinado, Anders Hagfeldt and Håkan Rensmo
The Journal of Physical Chemistry C, **115**, 19274–19279, 2011

II. **Influence of water on the electronic and molecular surface structures of Ru-dyes at nanostructured TiO_2**
Maria Hahlin, Erik M. J. Johansson, Rebecka Schölin, Hans Siegbahn and Håkan Rensmo
The Journal of Physical Chemistry C, **115**, 11996–12004, 2011

III. **Energy level alignment in TiO_2/metal sulfide/polymer interfaces for solar cell applications**
Rebecka Lindblad, Ute B. Cappel, Flannan O'Mahony, Hans Siegbahn, Erik M. J. Johansson, Saif A. Haque, Håkan Rensmo
Submitted

IV. **Electronic structure of TiO_2/$CH_3NH_3PbI_3$ Perovskite Solar Cell Interfaces**
Rebecka Lindblad, Dongqin Bi, Byong-wook Park, Johan Oscarsson, Mihaela Gorgoi, Hans Siegbahn, Michael Odelius, Erik M. J. Johansson and Håkan Rensmo
The Journal of Physical Chemistry Letters, **5**, 648–653, 2014

V. **The electronic structure of $CH_3NH_3PbX_3$ perovskites; the dependence on the halide moeity**
Rebecka Lindblad, Naresh K. Jena, Bertrand Philippe, Johan Oscarsson, Dongqin Bi, Hans Siegbahn, Erik M. J. Johansson, Michael Odelius and Håkan Rensmo
In manuscript

VI. **Energy level alignment in TiO_2/dipole-molecule/P3HT interfaces**
Erik M. J. Johansson, Rebecka Schölin, Hans Siegbahn, Anders Hagfeldt and Håkan Rensmo
Chemical Physics Letters, **515**, 146–150, 2011

VII. Energy level shifts in spiro-OMeTAD molecular thin films when adding Li-TFSI
Rebecka Schölin, Martin Karlsson, Susanna K. Eriksson, Hans Siegbahn, Erik M. J. Johansson and Håkan Rensmo
The Journal of Physical Chemistry C, **116**, 26300–26305, 2012

VIII. Controlling energy level positions in hole conducting molecular films by additives
Rebecka Lindblad, Johan Oscarsson, Kristofer Fredin, Susanna K. Eriksson, Hans Siegbahn, Erik M. J. Johansson and Håkan Rensmo
In manuscript

IX. Reactive ZnO/Ti/ZnO interfaces studied by hard x-ray photoelectron spectroscopy
Ronny Knut, Rebecka Lindblad, Sergey Grachev, Jean-Yvon Faou, Mihaela Gorgoi, Håkan Rensmo, Elin Søndergård and Olof Karis
Journal of Applied Physics, **115**, 043714, 2014

Reprints were made with permission from the publishers.

Comments on my own participation

The work done in this thesis has been the subject of team work. I have been the responsible person for preparing and performing the photoelectron spectroscopy experiments, treat the experimental data and writing the article in paper **I**, **III**, **IV**, **V**, **VII** and **VIII**. In paper **II**, **VI** and **IX** I have contributed with experimental work and discussions. (Note that in the early papers, my former family name Schölin is used.)

Extended bibliography

The following are publications to which I have contributed but that are not included in this thesis.

1. **Comparing surface binding of the maleic anhydride anchor group on single crystalline anatase TiO_2 (101), (100), and (001) surfaces**
Erik M. J. Johansson, Stefan Plogmaker, Lars Erik Walle, Rebecka Schölin, Anne Borg, Anders Sandell and Håkan Rensmo
The Journal of Physical Chemistry C, **114**, 15015–15020, 2010

2. **Solid state dye-sensitized solar cells prepared by infiltrating a molten hole conductor into a mesoporous film at a temperature below 150 degrees C**
   Kristofer Fredin, Erik M. J. Johansson, Maria Hahlin, Rebecka Schölin, Stefan Plogmaker, Erik Gabrielsson, Licheng Sun and Håkan Rensmo
   Synthetic Metals, **161**, 2280–2283, 2011

3. **Consequences of air exposure on the lithiated graphite SEI**
   Sara Malmgren, Katarzyna Ciosek, Rebecka Lindblad, Stefan Plogmaker, Julius Kühn, Håkan Rensmo, Kristina Edström and Maria Hahlin
   Electrochimica Acta, **105**, 83–91, 2013

4. **Low-temperature solution processing of mesoporous metal-sulfide semiconductors as light-harvesting photoanodes**
   Flannan T. F. O'Mahony, Ute B. Cappel, Nurlan Tokmoldin, Thierry Lutz, Rebecka Lindblad, Håkan Rensmo and Saif A. Haque.
   Angewandte Chemie International Edition, **52**, 12047–12051, 2013

5. **Linker unit modification of triphenylamine-based organic dyes for efficient cobalt mediated dye-sensitized solar cells**
   Hanna Ellis, Susanna K. Eriksson, Sandra M. Feldt, Erik Gabrielsson, Peter W. Lohse, Rebecka Lindblad, Licheng Sun, Håkan Rensmo, Gerrit Boschloo, and Anders Hagfeldt
   The Journal of Physical Chemistry C, **117**, 21029–21036, 2013

6. **High energy photoelectron spectroscopy in basic and applied science: Bulk and interface electronic structure**
   Ronny Knut, Rebecka Lindblad, Mihaela Gorgoi, Håkan Rensmo and Olof Karis
   Journal of Electron Spectroscopy and Related Phenomena, **190**, 278–288, 2013

7. **Atomic and electronic structures of interfaces in dye-sensitized nanostructured solar cells**
   Erik M. J. Johansson, Rebecka Lindblad, Hans Siegbahn, Anders Hagfeldt and Håkan Rensmo
   ChemPhysChem, *DOI: 10.1002/cphc.201301074*, 2014

8. **Understanding the effects of sputter damage in W-S thin films by HAXPES**
   Jill Sundberg, Rebecka Lindblad, Mihaela Gorgoi, Håkan Rensmo, Ulf Jansson and Andreas Lindblad
   Applied Surface Science, *DOI:10.1016/j.apsusc.2014.03.038*, 2014

9. **Enhancement of p-type dye-sensitized solar cell performance by supramolecular assembly of electron donor and acceptor**
   Haining Tian, Johan Oscarsson, Erik Gabrielsson, Susanna K. Eriksson, Rebecka Lindblad, Bo Xu, Yan Hao, Gerrit Boschloo, Erik M. J. Johansson, James M. Gardner, Anders Hagfeldt, Håkan Rensmo, Licheng Sun
   Scientific Reports, **4**, 4282, 2014

Contents

1 Introduction 11
1.1 Solar cells 11
1.1.1 Mesoscopic solar cells 11
1.2 This thesis 13
1.2.1 Outline of the thesis 14

2 Atoms, molecules, solids and light 15
2.1 The electronic structure of an atom 15
2.2 Molecules and solids 17
2.3 The interface between a solid material and a molecular film 19
2.4 Light-matter interactions 21

3 Photoelectron spectroscopy 23
3.1 The photoelectric effect and the basis of photoelectron spectroscopy 23
3.2 Core level spectra interpretation 25
3.3 Binding energy 26
3.4 Spin-orbit coupling 27
3.5 The chemical shift 27
3.6 Factors influencing the peak intensity 28
3.7 Varying the photon energy 30
3.8 X-ray absorption and resonant photoemission 32
3.9 Theoretical considerations 32

4 Experimental setups 35
4.1 Synchrotron radiation 35
4.2 The hemispherical analyzer 37
4.3 Measurements with hard X-rays 38
4.4 Measurements with soft X-rays 39
4.5 Practical considerations when measuring organic and semiconducting samples 39

5 Mesoscopic solar cells 43
5.1 The basic structure and function of the solar cell 43
5.1.1 The working principle 43
5.1.2 Energy levels and alignments 44
5.2 Basic solar cell characterization 46
5.2.1 UV-vis absorption 47

5.2.2 IV-measurements ... 48
5.2.3 IPCE ... 49
5.3 Light absorbers ... 49
5.3.1 Dye-sensitized solar cells ... 50
5.3.1.1 The influence of water on semiconductor/dye interfaces ... 51
5.3.2 Semiconductor-sensitized solar cells ... 54
5.3.2.1 Energy level alignment in TiO_2/metal sulfide/polymer interfaces ... 54
5.3.3 Perovskite solar cells ... 56
5.3.3.1 The TiO_2/Perovskite interface ... 57
5.3.3.2 The perovskite electronic structure ... 57
5.4 Hole conducting materials ... 58
5.4.1 Energy level alignment due to interfacial modification 60
5.4.2 Energy level shifts due to additives ... 62
5.4.3 Controlled doping of spiro-OMeTAD ... 64
5.4.4 Depth profiling of the mixed systems ... 64
5.5 Mesoporous TiO_2 ... 67
5.6 Conducting glass ... 68

6 Outlook ... 71

7 Populärvetenskaplig sammanfattning ... 73
7.1 Mesoskopiska solceller ... 73
7.2 Elektronspektroskopi ... 74
7.3 Experimentella resultat ... 75

References ... 79

1. Introduction

1.1 Solar cells

The sun is essential for life on this planet since it provides us with a lot of energy in form of heat, visible light and UV-radiation. A solar cell is a device that can convert some of this energy to electricity, through absorption of light and separation of charges. Once the solar cell is produced, the only input needed to produce electricity is light, and since there are no rest products in the process, solar cells are a good alternative for an environmental friendly and sustainable electricity production [1]. A rough calculation gives that if 0.1% of the Earth's total area was covered with solar cells that converts 10% of the incoming light to electricity, todays electricity consumption would be covered [2].

Starting 60 years ago with the development of the silicon solar cell [3], a lot of research has been focused on different kinds of solar cells based on various semiconductor materials, for example Si, GaAs, CdTe and CIGS (cupper indium gallium selenium) [4]. Solar cells including organic materials in different combinations with semiconductors is another family of devices. This includes for example mesoscopic solar cells and polymer/fullerene blends [2].

1.1.1 Mesoscopic solar cells

In the 1990:s, Michael Grätzel and coworkers did pioneering work on dye-sensitized photoelectrochemical solar cells including a wide band gap semiconductor, a dye and a liquid electrolyte [5]. The idea behind the dye-sensitized solar cell (also called a Grätzel cell) is that dye molecules absorb visible light and that the semiconductor and electrolyte transport charges. The method of making a large band gap semiconductor sensitive to visible light with the use of dye molecules was known earlier [6] but it was the introduction of a nanoporous semiconductor, giving a very large surface area, that enabled a functioning solar cell. Important motivations for the dye-sensitized solar cell are simple and low-cost production and also a high flexibility regarding materials and applications.

Today, the research field about dye-sensitized solar cells has grown tremendously [7] and other types of solar cells containing oxides and molecular materials have followed [8]. Replacing the liquid electrolyte with a solid hole conducting material gives a so-called solid state dye-sensitized solar cell, where the hole conductor can be an inorganic material or an organic polymer or

molecule [9, 10]. For light absorption purposes, the dye molecule can be replaced with quantum dots, making a quantum dot-sensitized solar cell [11], or a thin film of a semiconductor as in a semiconductor-sensitized solar cell (also called extremely thin absorber, ETA, solar cell) [2, 12]. There are also types where the light absorption and electron conduction take place in the same material, a mesoporous light-absorbing semiconductor [13]. All solar cells that are based on a nanoporous, or mesoporous, semiconductor may be grouped together as mesoporous or mesoscopic solar cells. The word mesoscopic reflects that the size domain relevant for this type of device is between microscopic and macroscopic, which in this case means in the range between several nanometers to micrometers.

Recently an organic-inorganic perovskite material was introduced as a thin absorber together with a solid hole conductor [14, 15]. These perovskite solar cells very quickly outperformed the efficiencies of the best dye-sensitized solar cell and is a rapidly increasing research field. The perovskite material is very diverse and can be used as a light absorber, as a hole conductor [16], as a combined light absorber and hole conductor [17] or as a combined light absorber and electron conductor [18]. It can be deposited onto a mesoporous semiconductor from solution, but can also be vapour deposited to form thin film configurations similar to the CIGS solar cell [19].

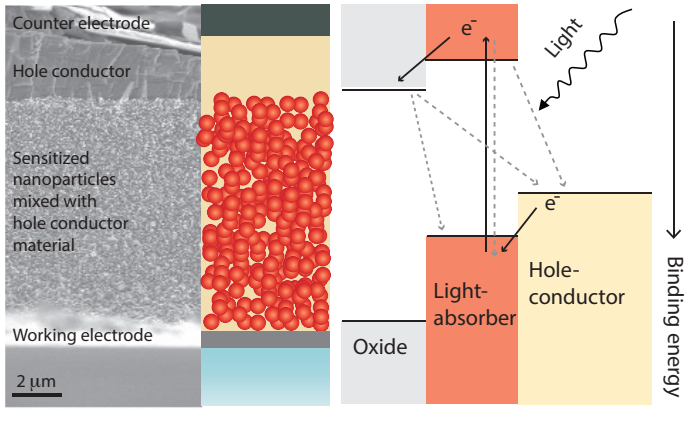

Figure 1.1. A SEM picture of a cut through a solid state mesoscopic solar cell (left), a sketch of the same solar cell (middle) and the energy levels in the different materials together with the working principle (right).

The basis for mesoscopic solar cells is nanoparticles of a semiconductor, typically TiO_2, covered with a light absorbing material (dye molecule, quantum dot, perovskite, etc.) see figure 1.1. When the solar cell is illuminated, an electron in the light absorbing material gets excited to a higher energy level in that material. This electron moves from the light absorber into the semiconductor and through the mesoporous network of semiconductor nanoparticles to a front contact. To reduce the oxidized light absorber, electrons are transferred from

the back contact through the liquid electrolyte or solid hole conductor. On the way from the front contact to the back contact, the electrons can be used to do work in an external device. The solar cell efficiency, *i.e.* the ability to convert light to electrical energy, varies between different types of solar cells and the highest values are in the order of 12% for liquid dye-sensitized solar cells [20], 7% for solid state dye-sensitized solar cells [21] and 15% for perovskite solar cells [19].

Figure 1.1 also shows different processes in the solar cell, including both the wanted processes, but also the unwanted backward reactions. Backward reactions do happen, but since they typically are slower than the favourable processes, the solar cell still works. Much work is therefore focused on how to make the favourable processes go faster and slow down the unfavourable.

1.2 This thesis

Even though there now is a basic understanding of the working principles of mesoscopic solar cells, there are still unanswered questions. The whole system is complex and to be able to characterize and understand it, many different methods are required. The charge separation, which is the core of conversion of light to electricity, occurs at the interfaces between the different materials in the device. Detailed atomic level electronic structure information of the materials and material interfaces allows basic understanding of functional interfaces and the development of mesoscopic solar cells. Photoelectron spectroscopy is a technique that can be used to study the electronic structures at the interfaces in the solar cell and in the different materials. This is very important since a good working solar cell requires a proper alignment between the energy levels in the different parts of the cell. When changing or modifying the materials, the energy levels and alignment may change, and understanding and controlling such effects is important for solar cell developments.

This thesis covers studies of materials from different types of mesoscopic solar cells and also different parts of the solar cell configuration. The different types include dye-sensitized, solid state dye-sensitized, semiconductor sensitized and perovskite solar cells. In these solar cells, the interface between a mesoporous semiconductor and a dye molecule, semiconductor or a perovskite is studied as well as thin films of hole conducting molecules and also the conducting glass itself. The overall aim is to get an atomic level understanding of the materials or the combination of materials and how different kind of modifications can change the electronic structure. Especially the energy level alignment between the different materials and how to modify this alignment has been the focus for this work.

The main experimental method has been photoelectron spectroscopy, which is an experimental method that uses X-rays to study *e.g.* the electronic structure and bonding in atoms, molecules and solids. Using lower photon energies, soft

X-rays, the technique is often referred to as PES (photoelectron spectroscopy) or XPS (X-ray photoelectron spectroscopy) and for higher photon energies, hard X-rays, the notations is HIKE (HIgh Kinetic Energy XPS) or HAXPES (Hard X-ray Photoelectron Spectroscopy). With soft X-rays, the technique is very surface sensitive and is thus useful to study the interaction of a molecule on a surface. Hard X-rays can on the other hand be used to study buried interfaces and the bulk electronic structure. In short, the main new experimental contribution from this thesis has been the development of methodology for measuring changes in energy level alignment with an element specific technique.

1.2.1 Outline of the thesis

The thesis starts with some basic knowledge about atoms, molecules and solids in chapter 2. Chapter 3 describes the main experimental technique, photoelectron spectroscopy, and chapter 4 the experimental conditions. Chapter 5 gives a more detailed description of the mesoscopic solar cells and how photoelectron spectroscopy can be used to characterise the materials for better understanding of their functional properties. This chapter also includes a summary of the experimental results.

2. Atoms, molecules, solids and light

Before moving into the core of this thesis, and to lay a ground for the coming discussion, I would like to give some background about the electronic structure of matter[1].

2.1 The electronic structure of an atom

Everything around us is made up by atoms with a positively charged nucleus surrounded by one or more negatively charged electrons. The magnitude of the positive charge defines which element it is. For example an element with eight positively charged protons in the nucleus (together with a similar number of uncharged neutrons) is regarded to be carbon. To be neutral, eight negatively charged electrons are circulating around the nucleus.

A particle in a circular motion is always accelerated towards the center of the path. According to classical mechanics such particle would loose some of its energy during the acceleration, by sending out radiation. In the atom, this would mean that the electron would move closer and closer to the nucleus and finally crash into it. This is fortunately not the case and we realise that the electronic motion can not be described by classical mechanics.

According to Bohr's model of the atom the electrons can only move in certain circular paths (shells) with fixed distances to the nucleus. In this description, both energy and radius are preserved. The electronic paths closer to the nucleus will be more affected by the positive charge compared to electrons further away. The closer the electron is to the nucleus, the more energy is therefore needed to remove it from the atom, which is described by a higher binding energy. Bohr's atomic model can be described by quantum mechanics where the electron is regarded as a wave rather than a particle. The distance to the nucleus can be kept if the electronic motion is a standing wave and the circumference equals an integer number of wavelengths. The electronic motion is then described by a wavefunction, Ψ, and the energy is found by using the Schrödinger equation:

$$H\Psi = E\Psi. \tag{2.1}$$

This equation may look simple and in one way it is. Nevertheless it can only be solved exactly for atoms with not more than one electron. For atoms with more

[1] For general references to this chapter see for example [22–24].

electrons you need approximations[2]. The Hamiltonian operator, H, describes the different contributions to the total energy, *i.e.*, the potential and kinetic energy (and different interactions). From the Schrödinger equation, which is an eigenvalue equation, you get the energy eigenvalues, E, which describes the energy state of a system. For the hydrogen atom the energies are obtained as

$$E_n = -\frac{1}{n^2}\frac{Z^2e^2}{2a_0}\frac{1}{4\pi\epsilon_0} \tag{2.2}$$

where Z is the nucleus charge, a_0 is the Bohr radius and n is the principal quantum number[3]. For each energy eigenvalue there is an eigenvector, the wavefunction Ψ_n, and these functions describe the orbitals where you can find the electrons. An orbital can be described as the spatial distribution where there is a certain propability density to find an electron.

In general, the principal quantum number is equal to the shell where the electron is found; it is labelled as a number where 1 is the shell closest to the nucleus. The number of electrons with a certain binding energy is however restricted; each shell therefore contains subshells with slightly different binding energy. These are described by the orbital angular momentum l, labelled *s*, *p*, *d*, *f*, *g*... depending on the symmetry of the orbital. In carbon, the electronic energy level that is closest to the core and that has the highest binding energy, is thus called the C *1s* electronic level or orbital. The two labels described so far are two out of four quantum numbers. In addition we have the magnetic quantum number and the electronic spin. Interactions between the spin and the orbital angular momentum (spin-orbit interaction) can give additional energy level splitting and is denoted with the spin quantum number as a subscript (as in S $2p_{1/2}$)[4].

According to the Pauli exclusion principle, two electrons can't have the same values on all four quantum numbers. This limits the number of electrons in a certain orbital. How the electrons are distributed among the energy levels is denoted in the electron configuration. As an example, the electron configuration of the sulphur atom is S $1s^2 2s^2 2p^6 3s^2 3p^4$, where the superscript denotes the number of electrons in each level.

The electronic binding energies ranges from 0–100000 eV. The lowest binding energies (up to approximately 20 eV for most elements) are found for the electrons furthest away from the nucleus: the valence electrons. These electrons can be delocalised over several atoms and are responsible for bonding between atoms. Above the valence levels, each element has very specific and well defined core levels and studies of their binding energy make it possible to distinguish different elements from each other. Such studies require a technique that uses energies comparable to the binding energy of the electrons. To

[2]Electron-electron repulsion can, for instance, be modeled with the central field approximation.
[3]The constants e and ϵ_0 is the electronic charge and the permeability in vacuum respectively.
[4]Spin-oribt interaction is described in more detail in chapter 3.4.

study the atom specific core levels, X-rays are therefore required, as is used in photoelectron spectroscopy, see chapter 3.

2.2 Molecules and solids

Combining atoms together to a molecule or a solid gives an overlap between the valence orbitals. This overlap is the basis for chemical bonding since it allows electrons to be shared between atoms and new molecular orbitals are formed. An illustration of this can be found in figure 2.1. The core levels are on the other hand localized and electrons from the core levels are not shared between atoms. The atomic character of the core levels remain after chemical bonding since they are not directly involved. Upon chemical bonding or other chemical reactions, the valence levels changes due to redistribution of electrons. Figure 2.1 also shows levels that are empty in the ground state, but can be occupied by *e.g.* excitation of electrons.

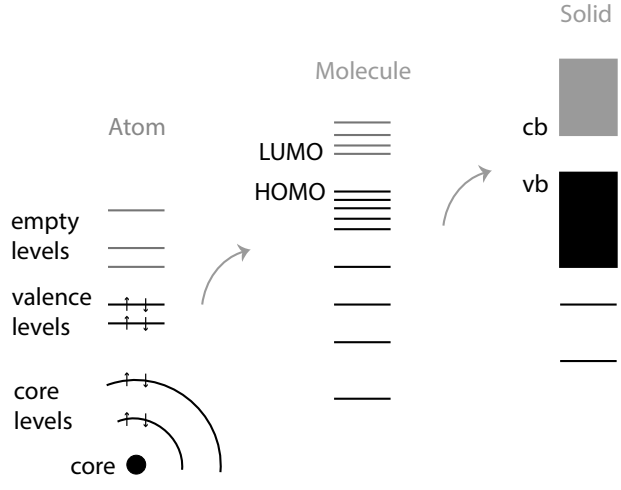

Figure 2.1. The energy levels in an atom, molecule and a solid (in this case a semiconductor with a gap between the valence and conduction bands).

The more atoms that are combined together, the more energy levels are found in the valence region, and the closer the levels are. For a solid with a large amount of interacting atoms, the highest occupied and the lowest unoccupied levels form bands, the valence and the conduction band respectively. For metals, the top band is partly filled and the highest occupied level is referred to as the Fermi level, E_F [5]. At room temperature, many electrons are thermally excited and these are the electrons responsible for electrical conduction. The excited electron leaves a level empty in the valence band, a so called hole,

[5]The definition of the Fermi level is the highest occupied level at the temperature zero Kelvin. Another word for the Fermi level is the chemical potential of a material.

which also contributes to the conduction. A totally full, or empty, band can not make any contribution to conductivity in the material.

The occupied and unoccupied bands (the valence and the conduction bands) in a semiconductor are separated by a gap with no energy levels, the bandgap[6]. This can be compared to the gap between the highest occupied molecular orbitals, HOMO, and the lowest unoccupied molecular orbitals, LUMO, in a molecule. The energy transition represented by an electron excited from HOMO to LUMO is of great importance for interactions between the molecule and, *e.g.* visible light.

The Fermi level is in this case within the bandgap and is defined as the energy where the probability of occupation of an energy level is exactly one half (as described by the Fermi–Dirac distribution function)[22]. The Fermi level is the electrochemical potential for electrons in a material and the position of the Fermi level relative the valence and conduction band edges is determined by the number of electrons in the conduction band and the number of holes in the valence band, *i.e.* the number of charge carriers on either side of the bandgap. In an ideal undoped semiconductor crystal, the Fermi level is in the middle of the band gap (at zero Kelvin). Adding electrons to the conduction band or removing electrons from the valence band can cause the Fermi level to move up or down, see figure 2.2. This can be achieved by impurities or imperfections introducing empty or occupied energy levels in the bandgap. This is referred to as doping of the semiconductor. Doping of conducting molecules are the topic in paper **VII** and **VIII**. The distance between the Fermi level, E_F and the transport level for holes, E_p, can be written as

$$E_F - E_p = -kTln\left(\frac{p}{N_p}\right) \tag{2.3}$$

where p is the density of holes and N_p is the density of states at the transport level. Equation 2.3 has its origin in semiconductor theory, but is also useful to describe molecular systems [25], although there are different ways to describe doping in molecular systems [25–29].

In a semiconductor at room temperature, there will be mobile charges both in the valence and conduction band (which one is more probable depends on *e.g.* doping). If electrically removing such conduction electrons, the average energy from where they are removed is at the Fermi level. The Fermi level is therefore the energy from where a conduction electron is taken out from a material and represents the free energy of the electrons[7].

In many descriptions, the energy where an electron is at rest directly outside a material is called the vacuum level. The energy difference between this

[6] An insulator is characterized by a very large bandgap over which thermal excitation is not possible.

[7] To remove the conduction electrons should however not be confused with the removal of core or valence electrons during photoelectron spectroscopy measurements since the latter are excited beyond the vacuum level.

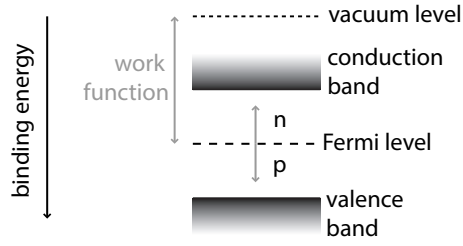

Figure 2.2. A schematic representation of important energy levels in a semiconductor. Adding extra electrons to the conduction band (n-doping) shifts the Fermi level upwards and adding extra holes to the valence band (p-doping) shifts the Fermi level downwards.

vacuum level and the Fermi level is defined as the work function, see figure 2.2. Since the binding energy of an electron in a material often is given with the Fermi level as zero binding energy, the amount of energy required to remove an electron from a material is the sum of the binding energy and the work function.

2.3 The interface between a solid material and a molecular film

As mentioned above, the vacuum level is often defined as the energy where an isolated electron is at rest outside a material. Far away from the surface (at an infinite distance) the vacuum level has the energy V_∞. Moving closer to the surface the vacuum level changes and just outside the surface it attains the value V_s. The surface vacuum level (V_s) can vary between different materials and also between different kind of surfaces of the same material. The latter is observed as a variation of the work function depending on the surface. The reason for the change of work function (or the vacuum level) for different surfaces can be due to a change of the surface charge. Depending on how the surface look like, the electronic cloud from the surface atoms can stick out from the core of the atoms and form a charged dipole layer at the surface. The strength of this dipole layer will affect the vacuum level just outside the surface and hence also the work function [26, 30–32].

If looking at a solid and a molecule far away from each other they will have the same vacuum level (V_∞). If brought in contact to each other, but without any transfer of charge between the solid and the molecule, the molecule will align its energy levels in such a way that the vacuum levels just outside the surfaces, V_s, of the molecule and solid attains the same potential, see (a) in figure 2.3. When this happens, all the electronic levels in the molecule will follow so that the distance between the V_s and the molecular electronic levels remains the same.

If a dipole layer is created at the interface (in addition to the dipole layer described above), the vacuum level at the interface may shift (as in figure 2.3(b)). A dipole layer can be formed by charge transfer across the interface or by chemical reactions at the interface. By putting a small molecule with a well defined dipole moment in between the solid and the molecular layer, it is also possible to control this vacuum level shift [33]. This is discussed in paper **VI**.

The work function of the inorganic solid and the molecular layer are usually not the same and hence, their respective Fermi level will not be at the same energy when the vacuum levels are aligned (with or without the shift in figure 2.3(b)). To compensate for the different Fermi levels, charges are rearranged at the interface in order to obtain equilibrium. Electrons will move to the material that has the larger work function (with the Fermi level at the lowest potential). This charge redistribution will affect the region closest to the interface; in the bulk of both materials the Fermi level will have the same position with respect to the valence and conduction levels (HOMO and LUMO) as before the charge redistribution. As a consequence of this, the energy levels will be shown with a bending of the electronic levels in the molecular layer close to the interface, sometimes referred to as band bending (figure 2.3(c)). Band bending will only happen (or will at least only be detectable) if there are enough mobile charges in the molecular layer and this requirement is fulfilled if the molecular layer is sufficiently thick. The charge separation in a pn-junction (as in a Si solar cell) is for example described by band bending at the interface between the p-doped and the n-doped material.

To summarize, the energy level alignment between two materials might be influenced by: dipole layers at the material surfaces giving different work functions; dipole layers created at the interface shifting the vacuum level at the interface; band bending in the semiconducting (or molecular) material. Moreover, the electronic structure obtained from the energy level alignment will define the properties of a functional interface, such as the key interfaces in mesoscopic solar cells

As an example, studies of a multilayer of a hole conducting molecule deposited onto single crystalline TiO_2 indicates a band bending in the molecular

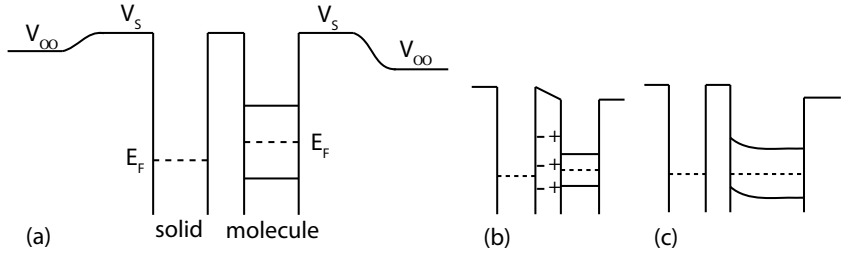

Figure 2.3. Energy levels in a solid and a molecular layer when brought in contact with each other (a), with a dipole layer in between (b) and with band bending (c).

film within the first nanometers from the interface [27]. Another example is the semiconducting nanoparticles in a mesoporous semiconducting film. It can be discussed that since theses nanoparticles are so small, no, or very small, band bending will occur inside these nanoparticles [2, 34, 35].

Photoelectron spectroscopy is a tool to experimentally investigate the electronic structures obtained from the alignment discussed above as shown in the present thesis. For example, in paper **VII** and **VIII**, changes of the Fermi level in molecular films are studied and to avoid effects from band bending, the more bulk sensitive technique HAXPES was used.

2.4 Light-matter interactions

What we usually refer to as visible light is a physical phenomena that more precisely can be described as electromagnetic radiation with a certain wavelength (visible light has the wavelength 400–700 nm). Electromagnetic radiation spans from Gamma and X-rays with short wavelength to ultraviolet, visible and infrared light at medium wavelength to micro and radio waves with long wavelength. All these different kinds of radiation consist of a transverse wave of oscillating electric and magnetic fields that moves at the speed of light. The different energies and wavelengths of the different part of the electromagnetic spectra are found in figure 2.4.

As described in chapter 2.1, an electron can be regarded as both a particle and a wave. In the same way, electromagnetic radiation can act both as a wave as described above, but also as a particle. This is called the wave-particle duality. In the particle-picture the energy of the light might be referred to as photon energies rather than wavelengths.

The particle description is very useful when discussing interactions between light and electrons in a material. When we say that light is absorbed by a mate-

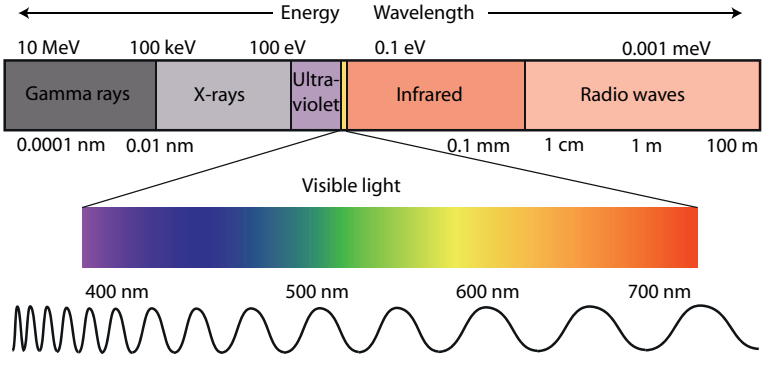

Figure 2.4. The electromagnetic spectra with wavelengths in nm and energies in eV.

rial, we actually mean that the energy in a photon is transferred to the material, which gets excited. For example can the energy be used to excite an electron to a higher energy level. The excited electron can fall back to its original level and at the same time a photon (or another electron) can be emitted. The energy of the emitted photon is then the same as the energy difference of the excited and the final energy level. The energy difference of the ground and excited states can create a voltage and can also be used to initiate an electric current, where the excited electron is transferred to an external contact. This is the basic principle of a solar cell. For the solar cell to work, there must be an energy gap between the energy levels occupied in the ground state and new levels occupied in the excited states, *i.e.* the solar cell must contain a semiconductor or a molecule with a HOMO–LUMO gap. The size of the gap corresponds typically to the energy in visible light for solar cells.

If a material is radiated with photons with very high energy, as in X-rays, the electrons can get enough energy to overcome its binding energy and leave the material. The emitted photoelectron then leaves a positively charged ion behind. Photoelectron spectroscopy is a technique that uses this behavior to identify materials and their chemical state, but more about this in chapter 3.

The system studied in this thesis (the solar cell), and the analysis method used (photoelectron spectroscopy), is thus based on interactions between light and electrons in a material. The differences being the energy of the photons and the destination of the excited electron.

3. Photoelectron spectroscopy

Photoelectron spectroscopy is a suitable method for element specific studies of surfaces and interfaces and has been the major experimental technique in this thesis. This chapter starts with the basic principles about photoelectron spectroscopy, including the photoelectric effect. Following are descriptions of the information that can be gained from the measurements.

3.1 The photoelectric effect and the basis of photoelectron spectroscopy

When an atom is irradiated with electromagnetic radiation, such as visible light, the energy in the light can be transferred to an electron in the atom causing the electron to be excited to a higher energy level. If the energy in the radiation is large enough for the electron to overcome it's binding energy, as for X-rays, the electron will be emitted from the atom. This phenomena is called the photoelectric effect and was first discovered by Hertz in 1887 [36] and later explained by Einstein in 1905 [37]. The process can be written as

$$h\nu + A \longrightarrow A^+ + e^- \tag{3.1}$$

where $h\nu$ is the photon energy in terms of the Planck constant h and the frequency ν. Depending on the energy of the radiation and the energy level in the atom that the electron originated from, the emitted photoelectron will have a different velocity, or kinetic energy. This can be written as

$$E_k = h\nu - \Phi - E_b \tag{3.2}$$

where Φ is the work function of the material of study and E_k and E_b are the kinetic and binding energies (referred to the Fermi level of the material) of the photoelectron. By detecting the kinetic energy of the emitted electron it is possible to calculate the electronic binding energy in a material[1]. This is what defines photoelectron spectroscopy and the method was developed by Kai Siegbahn and co-workers during the 1960s [38]. Since each element have specific energy levels, it is in this way possible to distinguish one element

[1] The kinetic energy detected by the spectrometer should not, however, be directly compared with the work function of the material, since the photoelectron gets influenced by the spectrometer. Instead, the binding energy scale can be calibrated using *e.g.* measurements of the Fermi level.

from another. To make it possible for the emitted electrons to reach the detector without colliding with molecules in the atmosphere, the experiments are conducted in vacuum.

Photoelectron spectroscopy is used to characterize the energy levels in atoms and can be used for gases, liquids and solids. During the photoemission process, electrons are removed from the matter under study. For general studies of gases or liquids, this is not a problem since the atoms or molecules continuously are renewed. For a solid on the other hand, electrons have to be transferred to the system so it can remain neutral. This requires samples with good conductivity (if not electrons are transferred to the sample via an electron gun).

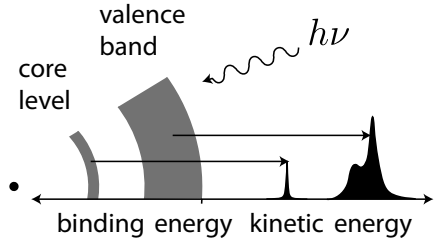

Figure 3.1. An illustration of an atom (to the left) and the corresponding XPS spectrum (to the right). [39].

According to equation 7.1, a lower kinetic energy of the emitted electron corresponds to a higher binding energy, *i.e.* an energy level closer to the atomic core. In photoelectron spectroscopy the number of emitted electrons are measured as a function of kinetic energy for a well defined photon energy. Each atomic level will in this way give rise to a peak in a photoelectron spectrum. An example spectrum can be seen in figure 3.1, where both the kinetic and binding energy axes are shown. Usually, experimental spectra are shown with the binding energy increasing to the left, as in the overview spectrum in figure 3.2. Each element has a unique spectrum and for a mixture of elements the resulting spectrum is, more or less, a sum of the individual spectra. The peak area can give quantitative information while the peak position can give information of the chemical state.

The above discussion relates to core levels that are localised on each atom and not directly involved in chemical binding. The valence electrons are on the other hand responsible for chemical bonding between atoms, and can be delocalised between many atoms. The valence levels measured with photoeletron spectroscopy can therefore be more difficult to interpret as they contain contributions from many atoms and elements. For the same reason can the valence levels give detailed information about chemical binding, chemical reactions and the density of states at the highest occupied levels.

The binding energy is generally given with the Fermi level as zero binding energy for solids and the vacuum level as zero energy for free atoms and molecules. For solids, the energy calibration is often achieved by direct measurements of the Fermi level. For a semiconductor, a metal in electric contact with the semiconductor can be used for binding energy calibration.

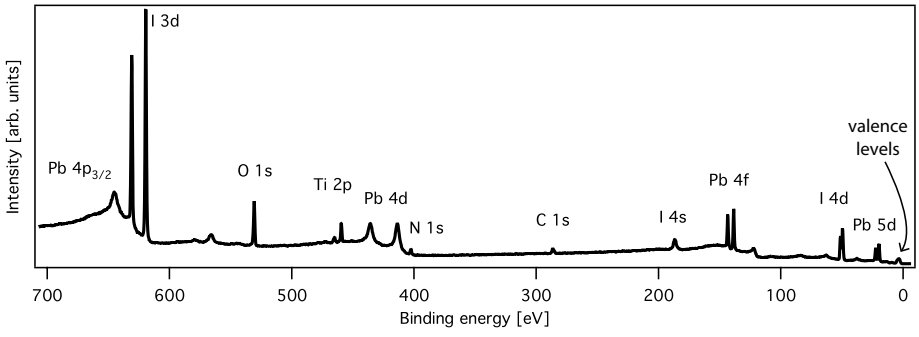

Figure 3.2. Overview spectra of a $CH_3NH_3PbI_3$ perovskite deposited onto mesoporous TiO_2 showing all elements in the sample.

3.2 Core level spectra interpretation

Photoelectrons that are elastically scattered on their way through the sample give a contribution to the background intensity. As can be seen in figure 3.2, the background intensity increases towards higher binding energies, with a step at every core level. This step-like background can be fitted with a Shirley function [40].

In the simplest picture the photoelectric effects gives an ionized atom in the ground state. It is however possible that the resulting ion is in an excited state (where the photoelectron excites valence electrons when leaving the atom). This will reduce the kinetic energy of the photoelectron giving a shake-up peak a few eV higher in binding energy compared to the main line. The photoelectron can also give enough energy to a valence electron to remove the latter from the atom. This is called a shake-off process, which also gives a peak at a higher binding energy.

When the core hole, created through the photoelectric effect, is filled with an electron from an outer energy level an Auger electron or a photon can be emitted. The Auger electron originates from an outer energy level and it's kinetic energy is the energy difference between the initial ion and the double charged ion. Auger electrons therefore have a constant kinetic energy when varying the photon energy, while photoelectrons have a constant binding energy. The difference between an Auger electron and a photoelectron is visualised in figure 3.3. Auger decay is dominating for lower photon energies while radiative decay dominates for higher photon energies.

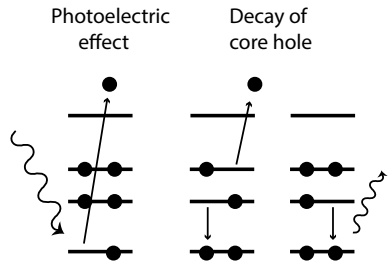

Figure 3.3. The creation of a photoelectron and a core hole (left) and subsequent core hole decay through emission of an Auger electron (middle) or a photon (right).

The core ionized state, created in the photoemission process, will eventually be filled with another electron. The ionized state has therefore a certain lifetime. This lifetime gives rise to an uncertainty of the energy of the state which will be seen as a broadening of the core level peak. The lifetime broadening gives a Lorentzian lineshape. In a photoelectron spectroscopic experiment there are also other sources of line broadening that limits the resolution, *e.g.* from the spectrometer or the X-ray source. The experimental broadening is described by a Gaussian lineshape. The total lineshape can therefore be modeled by a convolution of a Lorentzian and a Gaussian, called a voigt function. In metals the photoelectrons can interact with conduction electrons and thus loosing some energy, giving an assymetric lineshape on the high binding energy side of the main line, better described by a Doniach–Šunjić line profile [41].

3.3 Binding energy

The atomic core level binding energy is dependent on the energy difference between the neutral initial state and the core-ionized final state of the atom. This can be described by

$$E_B = E_{tot}(N-1) - E_{tot}(N) \tag{3.3}$$

where E_{tot} describes the total energies of the initial state with N electrons and the final state with N-1 electrons. For a given orbital k, the binding energy $E_B(k)$ is described by the initial and final total energies for that orbital.

To calculate total energies are however a difficult task and different approximations are therefore applied. The simplest way to calculate the binding energy is by assuming that no rearrangement of the remaining electrons occur during the process, which is called Koopman's theorem. In this approximation the Schrödinger equation (2.1) is solved using Hartre–Fock wavefunctions to calculate the ground-state orbital energies, ϵ_k [42]. This calculation also assumes that there is no interaction between the photoelectron and the system, called the Sudden approximation.

The final state has however lost an electron and therefore the electrons will not screen the nuclear charge as effectively as before. This creates relaxation of the remaining electrons to adjust to the new situation. The ground state orbital energies can therefore be corrected with the relaxation energy, E_R, and the binding energy can be described as

$$E_B(k) = -\epsilon_k - E_R. \tag{3.4}$$

Another approximation uses the fact that the removal of a core electron can be approximated with an extra proton in the nucleus. This is the Z+1 approximation and can, together with thermodynamic data, be used for a relatively easy estimation of the binding energy[2] [42].

3.4 Spin-orbit coupling

When an electron with relativistic velocity, moves in an electrical field, it will experience an effective magnetic field. The magnetic moment of the electron, can couple to this magnetic field, causing a perturbation of the energy levels of the atom. Since the electronic motion is described by the orbital angular momentum (the quantum numbers n and l) and the electrons' magnetic moment is proportional to the spin, this perturbation is called a spin-orbit interaction. Spin-orbit interaction causes a splitting of an electronic level, where the perturbation energy depends on whether the angular momentum is paralell or antiparalell to the spin [24]. This occurs for electrons in orbitals with an orbital angular momentum larger than zero (*i.e.* all orbitals except s-orbitals). The intensity relation between the two spin-orbit splitted lines is dependent on the amount of states in each.

For example, a p-orbital can be either $p_{1/2}$ or $p_{3/2}$, where the number of electrons in the $p_{1/2}$ state is half that of the $p_{3/2}$ state. An example can be seen in figure 3.4 displaying the Ti 2p core level in TiO_2. The intensity of the Ti $2p_{1/2}$ level is half that of the Ti $2p_{3/2}$ but due to an extra decay channel of the Ti $2p_{1/2}$ level (a Coster–Kronig transition [43]), this level has a shorter lifetime and thus a broader Lorentzian contribution compared to Ti $2p_{3/2}$.

3.5 The chemical shift

When combining two atoms together to form a molecule, the energy levels in the atom will be affected. This is most noticeable for the valence levels where the atomic orbitals in the atom will be combined to molecular orbitals when

[2]This is done in a so called Born–Haber cycle where the calculations includes removal of an atom from the material and ionization of that atom before it is put back in the material again [42].

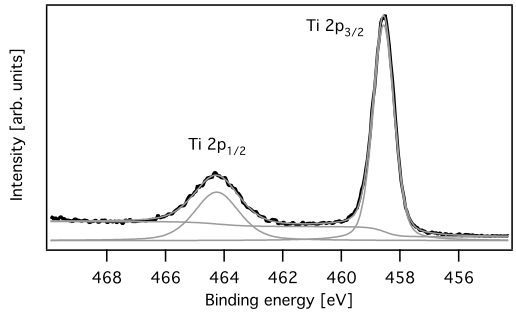

Figure 3.4. The Ti 2p core level in mesoporous TiO_2 measured with a photon energy of 4000 eV. Voigt profiles and a shirley-type background are used for curve fitting.

forming a molecule. These molecular levels can differ much compared to their corresponding atomic levels and there is in general large contribution from many atoms. The core levels on the other hand will remain more intact when a molecule is formed, but they can still be affected by the surrounding atoms. This is seen as a chemical shift of the core level [38], which is dependent on the nature of the surrounding atoms.

As equation 3.3 can be used to calculate the binding energy of a core level, it can also be used to calculate the chemical shift, ΔE_B, between two compounds A and B, as $\Delta E_B = E_B(A) - E_B(B)$. Using the Z+1 approximation in a Born–Haber cycle is another way to estimate the chemical shift.

An example of when a chemical shift occurs is the removal of a valence electron (through for example a chemical reaction), which will change the charge around a core electron. The core electron therefore feels a stronger Coulomb interaction to the nucleus resulting in a larger binding energy.

Changing the surrounding atoms also changes the charge around the core electrons. In a simple picture, a binding to a more electronegative atom will therefore cause the core level to shift to higher binding energies and a less electronegative atom gives a chemical shift to lower binding energies. An example can be seen in figure 3.5 for the C 1s level, where *e.g.* fluorine gives a large chemical shift due to its electronegativity. The nature of the chemical shift gives thus information about chemical bonding in a molecule. There can also be a chemical shift between surface atoms and bulk atoms in a solid due to the different amount of neighbouring atoms.

3.6 Factors influencing the peak intensity

The intensity of a photoemission line is determined by the transition probability between the initial and final state wavefunctions. This can be described by

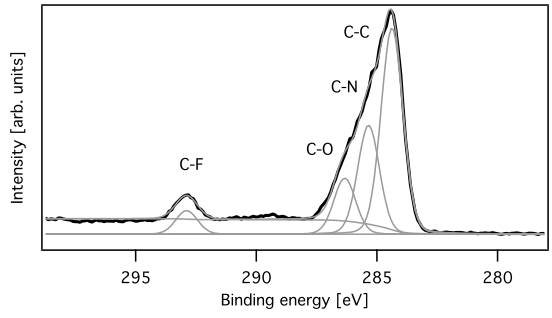

Figure 3.5. The C 1s core level of a mixture of spiro-OMeTAD and Li-TFSI measured with a photon energy of 2010 eV showing the chemical shifts when carbon bonds to the other elements[44]. The amounts of the different kinds of carbon is reflected by the intensities of the different contributions to the total carbon signal.

Fermi's Golden Rule [23, 42]

$$w_{fi} = \frac{2\pi}{\hbar}|\langle\Psi_f|H|\Psi_i\rangle|^2\delta(E_f - E_i - h\nu) \tag{3.5}$$

where H is the Hamiltonian describing the interaction between the electromagnetic radiation and an electron, and Ψ_i and Ψ_f are the wavefunctions of the initial and final states with energy E_i and E_f respectively. If using the correct wavefunctions for the initial and final states and the dipole operator as H, Fermi's Golden Rule gives a correct description of the photoelectron process, however approximations are needed to solve it [42]. From this equation follows that the distribution of emitted photoelectrons is proportional to the initial density of states.

In practical photoelectron spectra, several parameters are responsible for the transition probability and therefore the intensity, I, of a photoemission line, see equation 3.6 [45]. These parameters are the surface concentration of the material under study, n, the photon flux, f, the photoionization cross section of the process, σ, the angular efficiency factor of the instrumental arrangement, θ, the mean free path of the electrons, λ, the area of the sample from where photoelectrons are detected, A, and the analyzer transmission, T.

$$I \propto nf\sigma\theta\lambda AT \tag{3.6}$$

The more of a specific element on the sample surface, the more intense will the peak be (an example of this can be seen in figure 3.5). Due to the surface sensitivity of the technique, elements closer to the surface will also give a larger contribution to the peak.

The probability that the photoelectric effect will occur when a material is irradiated with X-rays is called the photoionization cross section. The subshell photoionization cross section combines the transition probability for the given

photon energy and the density of states of the initial and final state of the interaction [42]. The cross section is dependent on the photon energy and the material and orbital of interest. In general, the cross section for a given subshell decreases with increasing photon energy, even though localized maxima and minima can be found [46]. The rate of decrease differs between different elements and subshells. This can be used to identify the contribution from each element *e.g.* in a mixed molecular valence level. To a first approximation, metals and heavier elements have higher cross section for higher photon energies compared to lighter elements such as carbon and nitrogen. To map out the metallic contribution to a mixed valence levels, high photon energies are therefore useful [47].

When using polarized light, as in a synchrotron, the polarization direction versus the orbital symmetry can give additional dependence to the cross section [46]. This is true for free atoms and is a good approximation for gases and liquids. If measuring a solid sample with a high photon energy, giving bulk sensitive measurements, elastic scattering of the outgoing electrons can be large enough to give an isotrop electron emission and thus changing the symmetry dependence [48].

3.7 Varying the photon energy

Photons can travel far in a material before they interact with an electron, the negatively charged electrons on the other hand, interacts very easily with the positive cores or other electrons. This interaction limits the distance electrons can travel through a material. The average distance the electrons travel without energy loss is called the electronic mean free path, or the escape depth. For a certain electronic level, the mean free path depends on the kinetic energy of the electron, which depends on the photon energy where a higher photon energy gives a longer mean free path. The mean free path as a function of the kinetic energy measured for various materials show a universal curve, see figure 3.6. From this curve it can be seen that the shortest mean free path are found for a kinetic energy of 50 eV. On both side of this minimum, the mean free path increases. For very low kinetic energies however, material effects can cause deviations from the universal curve [42].

Varying the energy of the incoming radiation provides therefore a further source of information in the measurements. One parameter that can be tuned is the depth from where the electrons will escape the material, due to the limited electronic mean free path. With a relatively low photon energy, the photoelectrons will get low kinetic energy, and hence, will not be able to travel far in a material. Higher photon energies gives higher kinetic energies and increases the depth from where the electrons can be emitted and the measurement becomes more bulk sensitive.

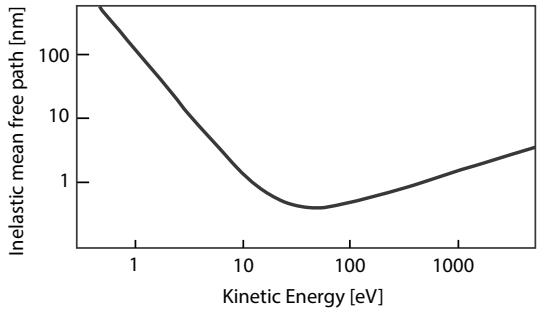

Figure 3.6. Inelastic mean free path of electrons as a function of the kinetic energy [49].

The relative cross sections also vary with energy, which means that the relative contribution from different elements can be tuned. This type of information coupled to theoretical calculations leads to detailed insight into the electronic structure of the studied material.

In relatively simple molecules in gas phase, intensity variations as a function of photon energy has been observed. This was explained by interaction of neighbouring atoms giving a variation of the cross section for different atoms [50]. For a larger molecule adsorbed to a surface, this kind of cross section variations was not observed [51].

The field of photoelectron spectroscopy has been divided into subgroups depending on the kind of radiation used. UV light, for example, will only be able to emit electrons from the valence levels, but is particularly useful for this purpose. Photoelectron spectroscopy based on UV light is commonly called UPS (UV Photoelectron Spectroscopy). Going into the X-ray regime, the X-rays can be divided into soft X-rays with photon energies between 100–2000 eV, and harder X-rays with photon energies above 2000 eV [52]. When using the first kind of X-rays the technique is called XPS (X-ray Photoelectron Spectroscopy). For hard X-rays the technique is called HAXPES (HArd X-ray PhotoElectron Spectroscopy) or HIKE (HIgh Kinetic Energy photoelectron spectroscopy). The acronyms PES (PhotoElectron Spectroscopy) or ESCA (Electron Spectroscopy for Chemical Analysis) are also used as common names for the technique. It can be mentioned that the first photoelectron spectroscopy measurements actually were HAXPES measurements, since the first instrument was equipped with an X-ray tube with Cu Kα radiation giving a photon energy of 8048 eV [38]. The real sucess of this technique came however first with the development of electron spectrometers that allowed measurements of high kinetic energies with resonable resolution and transmission [52]. Harder X-rays are very useful to detect electronic levels with very high binding energy, and also to detect the bulk of a material. It should however be mentioned that when deep core levels with very high binding energy are monitored, the measurements becomes surface sensitive since the kinetic energy of the pho-

toelectrons is low. UPS and XPS are more surface sensitive techniques where depths to a few nanometers can be seen, whereas HAXPES can be used to probe up to 20 nm into the material (and even deeper for porous materials) [53]. In this thesis work, XPS and HAXPES are used in combination.

3.8 X-ray absorption and resonant photoemission

If an incoming photon has the same energy as the binding energy difference between a core level and an unoccupied level, an excitation can occur where the photon is absorbed by the atom. This process leaves the atom with a core hole, which is rapidly filled with an electron from an outer level. In this decay a photon or an Auger electron leaves the atom (compare to the decay processes in figure 3.3). For core levels with relatively low binding energy, decay through Auger emission is more probable, while for core levels with higher binding energies radiative decay dominates.

In an X-ray absorption experiment, the amount of emitted Auger electrons (or photons) is measured while the photon energy is scanned over the absorption threshold. At specific energies corresponding to absorption edges there will be higher probability of absorption and also for releasing an Auger electron (or photon) resulting in a peak in the X-ray absorption spectra. In this way the unoccupied levels are probed. If studying the absorption close to an edge, the technique is usually called NEXAFS (near edge X-ray absorption fine structure). X-ray absorption is an element specific technique since the core hole and the unoccupied levels are found in the same atom.

In resonant photoemission spectroscopy (also called resonant Auger spectrosocpy) the photon energy is also scanned over an absorption edge, but instead of measuring the emitted Auger electrons as in X-ray absorption, the valence levels are measured for each photon energy[3]. Due to a higher cross section at the resonance (where the photon energy matches the excitation from a core level to an unoccupied level) there will be an enhancement in the parts of the valence band spectra containing contributions from the atom where the resonance occured. In this way it is possible to map different atomic contributions to the often complex valence spectra.

3.9 Theoretical considerations

A photoelectron spectrum can be well modelled by theoretical calculations and a combination of experiment and theory is therefore a valuable tool for a detailed understanding of the electronic structure. As the electrons are best described by quantum chemistry, the theoretical methods includes solving the

[3] In the same way as in normal photoelectron spectroscopy.

Schrödinger equation (equation 2.1). For a system with many electrons, this is done numerically and by using different approximations.

One way to calculate the electronic structure of matter is by using Density Functional Theory (DFT) [54]. The method was introduced in the 1960's by Hohenberg, Kohn and Sham [55, 56] and is a well used method today. The idea behind the method is that the Hamiltonian (used for solving the Schrödinger equation) can be described by the electron density. The electron density is the probability to find an electron in a certain volume element and provides a simplified way to describe the energy of a system compared to a many electron wave function. The total ground-state energy can then be described by functionals of the electron density, including the kinetic energy and the interaction energy. Applying a variational principle, the minimum value of the functional can be found, which corresponds to the ground state density. The calculation starts with an initial guess of the density and in an iterative procedure the orbitals that minimizes the total energy are found.

The perovskite structures described in this work (see chapter 5.3.3 and paper **IV** and **V**), that are used as light-absorbers in mesoscopic solar cells, are modelled by means of DFT. The positions of the atoms was exctracted from reported crystal structures and were geometry optimized. The electronic structure was then calculated with DFT, where the different kind of atoms were described with different potentials. One-electron wavefunctions (Kohn-Sham orbitals) was used to model the photoionization process. The result shows the electronic density of states (DOS). The partial density of states (PDOS) of each atomic contribution was extracted through an analysis of the atomic charges (a Mullikan analysis). For chemical shifts, the Z+1 approximation was also used. To match the experimentally measured photoelectron spectra, a Gaussian width was adapted to all calculated energy levels. The results include detailed analysis of the valence levels and understanding of chemical shifts observed for different perovskite materials.

4. Experimental setups

Shortly, the setup for photoelectron spectroscopy measurements contain an X-ray source, an analyser and some vacuum compatible tools for sample handling. The major part of the experimental work in this thesis is performed at two different synchrotrons: MAX-IV in Lund and BESSY II in Berlin. Here follows a description about a synchtron radiation source and the beamlines where the experimental work took place together with some basis about how to detect the photoelectrons. The chapter ends with a discussion about sample treatment.

4.1 Synchrotron radiation

Photoelectron spectroscopy is a technique that requires X-rays with a well defined photon energy. X-rays can be produced by electrons hitting an anode as in an X-ray tube, or by accelerating electrons as in a synchrotron. The light from a synchrotron is tunable, polarized, has high brilliance and can be focused to a narrow beam, thus very useful for X-ray photoelectron spectroscopic studies.

The basic principle of synchrotron radiation is that charged particles (typically electrons) emit radiation when accelerated [57]. The electrons are accelerated to relativistic speed (that is, close to the speed of light) and stored in a nearly circular ring, called the electron storage ring, see figure 4.1. The storage ring consists of straight sections between strong magnets that bend the path of the electron beam. In the transverse acceleration caused by the bending magnet, the electrons emit radiation. This is the simplest way to create synchrotron radiation [58]. The radiation can contain energies in a broad spectrum from far IR to hard X-rays (compare with figure 2.4), a monochromator is then used to select the desired photon energy.

The more the electrons are bent, the higher the photon energy of the produced light (the shorter the wavelength). Since the electrons need to continue in its nearly circular path, there is a limit in the strength of the bending magnet; a too strong magnet would cause the electrons to bend out of their orbit. If a series of magnets are used in an array, the original direction of the electrons can be restored and stronger magnets can be used. As a consequence of the many turns the electrons make in a magnetic array, the brilliance of the light increases (brilliance is photon flux and beam size combined, a high brilliance gives a high intensity in a small spot). Such a device is called a wiggler or an undulator [59], the difference being that in an undulator the electrons are

bent more times giving a higher brilliance. In an undulator there are also sharp intensity peaks corresponding to positive interference between the electrons. A wiggler on the other hand can use stronger magnetic fields that produces more energetic photons. Wigglers and undulators can be placed in the straight sections of a synchrotron storage ring, between the bending magnets.

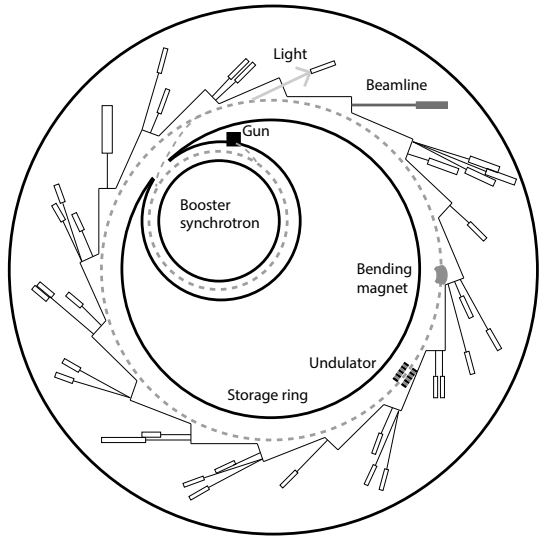

Figure 4.1. A schematic sketch of a synchrotron where an electron gun injects electrons to the booster ring where they are accelerated to relativistic speed after which they are injected to the storage ring. The synchrotron BESSY II is the model for this figure.

The photon energy range of the produced light is not only dependent on the magnitude of the acceleration, but also on the energy, or speed, of the electrons in the storage ring [59]. The higher the energy of the electrons, the higher photon energy will be created. To keep high energy electrons in a circular path, strong magnetic fields is required, alternatively the radius of the storage ring is made large.

In addition to this, different types of monochromators are suitable for specific energy ranges; a grating monochromator works for an energy range of lower photon energy whereas a crystal monochromator is better suited for higher photon energies. One definition of hard X-rays is the energy where a grating no longer works as a monochromator, which is at energies above 2000 eV [52]. Instead, the photon energy is set by bragg reflection in a single crystal of for example Si.

The generated light leaves the storage ring through a beamline where it passes the monochromator and where mirrors, gratings and slits focuses the beam on the sample. The end station with the analysis chamber is located at the end of the beamline where the photoelectron spectroscopic experiments are performed.

4.2 The hemispherical analyzer

One way of detecting the kinetic energy of the emitted photoelectrons is by using an hemispherical electron energy analyzer [42]. Another way is to measure the time it takes for an electron to pass through the spectrometer, as in a time-of-flight-spectrometer [60]. The former type is used for all photoelectron spectroscopy measurements in this thesis and a hemispherical spectrometer can be seen in figure 4.2.

The idea with a hemispherical spectrometer is to let the photoelectrons pass between two hemispherical electrodes where the trajectory of the electrons is dependent on their kinetic energy. At the other end of the hemisphere, the electrons are dispersed on a multichannel detector. Only electrons with a kinetic energy close to the one following the radius of the central trajectory (the pass energy, E_p,) between the hemispheres will hit the detector. A system of electrostatic lenses placed before the entrance to the hemisphere is used to accelerate or retard the electrons emitted from the sample, to select an energy window that can pass through the hemisphere. The pass energy together with the entrance slit width (S) and the radius of the analyzer (R_0) determines the resolution of the spectrometer according to equation 4.1.

$$\Delta E = E_p \frac{S}{2R_0} \tag{4.1}$$

During a measurement, the pass energy is set to a specific value, but the acceleration or retardation voltages of the electron lenses are varied in order to scan over all possible kinetic energies. For each particular energy, the number of electrons hitting the detector are counted and saved, and later integrated to a spectrum.

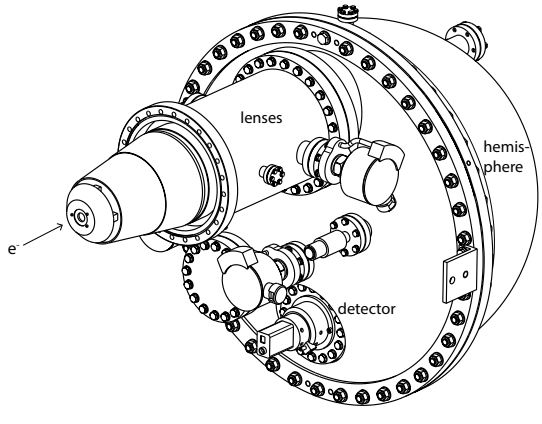

Figure 4.2. A hemispherical spectrometer of type Scienta R4000 10keV. The electron passes through a system of electrostatic lenses and the hemisphere before hitting the detector. Figure courtesy of VG Scienta.

4.3 Measurements with hard X-rays

Photoelectron spectroscopic experiments using hard X-rays were performed at the HIKE end station at beamline KMC-1 at BESSY II in Berlin [53, 61]. The photons are created by a bending magnet at this beamline. The beamline is further equipped with a crystal monochromator with three different crystals: Si(111), Si(311) and Si(422). Each crystal is suited for a specific photon energy range and altogether they can provide photon energies between 2–12 keV. Detection of photoelectrons is made by a hemispherical Scienta R4000 10 keV spectrometer configured for high kinetic energy photons.

Measurements are usually performed with the photons hitting the sample at a grazing incidence angle. The spectrometer is in a direction that is close to the surface normal of the sample (the beam and the spectrometer are at a 90 degree angle). This configuration makes the measurements bulk sensitive. In figure 4.3 the HIKE end station is shown. The X-ray beam is coming from the right in the figure. Samples are introduced via a load-lock chamber and transferred in vacuum to the measurement position in the analysis chamber. Possible *in situ* preparations include Ar ion sputtering and heating.

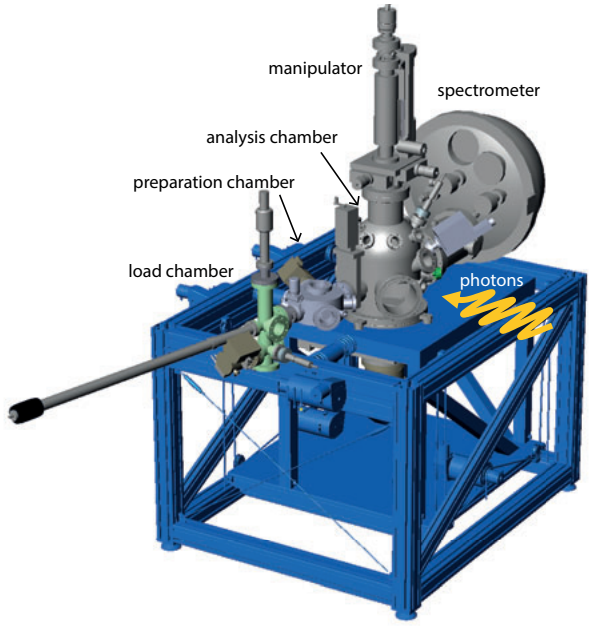

Figure 4.3. A figure showing the HIKE end station at KMC-1 at BESSY II.

HAXPES can be used to study bulk electronic properties and buried interfaces. In papers **VII** and **VIII**, the bulk sensitivity is used to minimize the effect of the surface, to avoid detection of surface contaminants and possible band bending at the sample/vacuum interface. For molecular materials that are difficult to deposit *in situ*, this is very useful. In papers **IV**, **VI** and **IX**, the

bulk sensitivity was used to study buried interfaces. As mentioned in chapter 3.7, higher photon energies can also be used to highlight the contribution of a certain element that has a relative high photoionization cross section at high energies. This was used in papers **IV** and **V** when measurements of the perovskite compounds $CH_3NH_3PbI_3$ and $CH_3NH_3PbBr_3$ were compared to theoretical calculations.

4.4 Measurements with soft X-rays

Photoelectron spectroscopy experiments with photon energies between 100 – 1000 eV were carried out at beamline I411 at the Swedish national synchrotron facility MAX-lab in Lund [62]. This beamline is equipped with an undulator for light generation and a plane grating monochromator selects the desired photon energy before the beam reaches the sample. The analyzer is a hemispherical Scienta R4000 wide angle lence spectrometer. This beamline can be used for various kinds of experiments and the setup can accordingly be changed as to be used for gaseous, liquid and solid samples. For the experiments on solid samples used in this thesis work, a transfer chamber and a manipulator for sample movement is placed on top of the analysis chamber, see figure 4.4. To this transfer chamber a smaller chamber, used for fast loading of *ex-situ* samples, is mounted together with a magnetic rod that can move the samples from this load-lock chamber to the transfer chamber. Measurements are typically performed with an angle of 30 degrees between the spectrometer and the surface normal of the sample.

The lower photon energies accessible by this beamline are particularly useful to study valence bands and band gap states. Interfaces of semiconductors and a light absorbing material can be studied in great detail if only the latter material is thin enough (this is always the case for *e.g.* dye molecules). In paper **III**, we show that is also is possible to study interfaces of a mesoporous semiconductor, a metal sulphide and a polymer.

4.5 Practical considerations when measuring organic and semiconducting samples

All samples measured in this work relates to different kinds of mesoscopic solar cells and here I would like to discuss some general aspects to take into account during measurements of these kind of samples. More detailed descriptions of sample preparation for each type of solar cell configuration are however found in chapter 5.

The name semiconductor imply that the material is only partly conducting. If the conduction of electrons through the material in the sample is slower

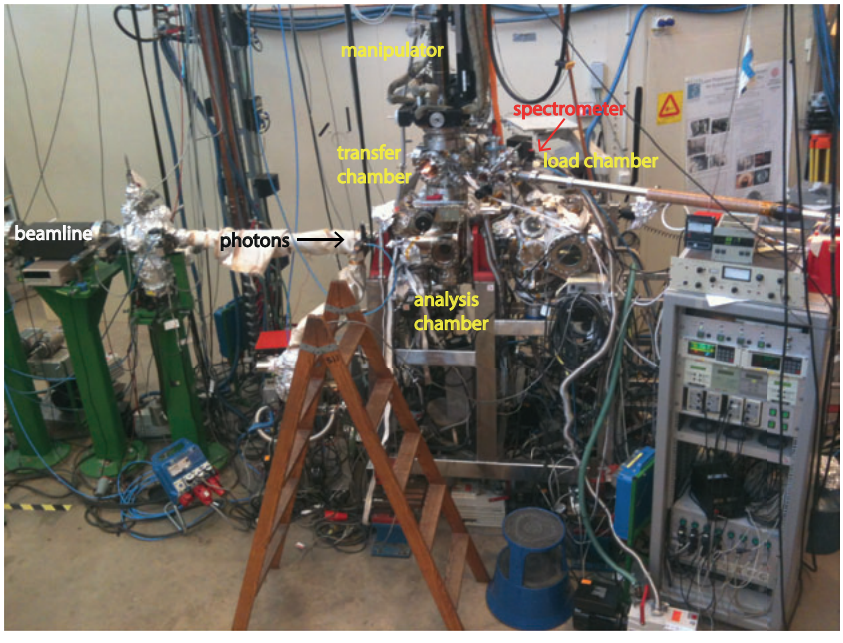

Figure 4.4. The setup at I411 at MAX-lab with the beamline to the left, the analysis and transfer chambers together with the manipulator in the middle and the load-lock chamber and the magnetic rod to the right. Hardly visible behind the analysis chamber is the spectrometer.

than the removal of photoelectrons, the material will be positivley charged during photoelectron spectrosocpy measurements. This will induce a shift of the photoelectron lines towards higher binding energy in a spectrum. The charging is generally larger directly after starting radiating the sample with X-rays, but eventually reaches a steady-state where the charging can be controlled. Variations in X-ray intensity changes this steady-state. Most of the photoelectron spectroscopy measurements in this work have been conducted at a synchtrotron that was running in decay-mode where the X-ray intensity decreases with time[1], thus changing the charging over time. One way to energy calibrate the measurements of poorly conducting samples is to use an internal binding energy reference. A core level in a mesoporous semiconductor can for example be used to binding energy calibrate the electronic levels from an adsorbed dye molecule or light absorbing semiconductor.

An internal reference is however not always possible. An example is the studies of thin films of hole conductors studied in this thesis, where the aim was to compare the electronic binding energies in the bulk material before and after the addition of a Li-salt or a Co-complex. The core levels of the hole conductor could in this case not be used as an internal binding energy reference

[1]Some of the later experiments at BESSY have however been performed during top-up mode, where the X-ray intensity is stable over time.

since the goal was to follow shifts of the core levels themselves. A metal in electric contact with the molecular film can instead be used to reference the binding energy of the molecular material to the Fermi level. To avoid erronous results due to binding energy shifts caused be charging, possible charging can be monitored by decreasing the X-ray intensity while following the binding energies of core levels in the molecular material relative the reference metal. A core level shift of 0.05 eV or less when decreasing the X-ray intensity by half was in this work assumed to be sufficient to avoid erronous results due to charging. If necessary, the X-ray intensity was decreased until this requirement was fulfilled.

Light absorption and charge separation in a mesoscopic solar cell are dependent on the relative energies of valence and conduction band edges. Even though photoelectron spectroscopy is a suitable technique for determining the binding energy of the valence band edge relative the Fermi level, the exactness in which this can be done can be discussed. If the valence band edge would have been a step function the determination of its binding energy would have been easy. In reality the edge is more a slope, and the binding energy of the edge is usually defined as where a straight line with the same angle as the slope intercepts with the x-axis. How to draw this straight line is however not unambiguously defined. In this work, the energy level alignment is therefore given as the distance (binding energy difference) between valence band edges, rather than to give a direct binding energy of the edge. In a molecular material, the HOMO is a better description of the highest occupied level than a conduction band edge. The experimental difference is that the HOMO often can be seen as a distinct peak, and not a slope. In this case, a peak fit can give the binding energy of the HOMO level.

5. Mesoscopic solar cells

This chapter includes a more detailed description of the function of mesoscopic solar cells. The chapter starts with a basic description of the function and how to characterize the basic solar cell properties. The different materials in the device are then treated in more detail according to their function: light absorbing, hole conducting or electron conducting. In this latter part the sections start with a general description of different types of devices, which is followed by a more detailed discussion of the most important experimental results from this thesis.

5.1 The basic structure and function of the solar cell

5.1.1 The working principle

As mentioned already in the introduction, the basic structure for the mesoscopic solar cell investigated in the present thesis is a mesoporous network of a semiconductor material, where oxides are the most widely used [7]. Adsorbed to the semiconductor surface is a monolayer of dye molecules or a thin film of a small band gap semiconductor (the light absorber). A hole conducting molecule (in a solid-state device), or a liquid electrolyte (in a liquid device), fills the mesoporous network. As a substrate for the mesoporous oxide film and as a transparent conducting front electrode, glass with a conducting film (FTO or ITO) is used. The back contact is either another piece of conducting glass (for liquid devices) or a thin film of a metal (for solid-state devices) that is usually deposited through evaporation.

The working principle of a mesoscopic solar cell is described in figure 5.1. The light absorber absorbs the incoming light and the energy in a photon is used to excite an electron. This absorption is often represented as an electron jumping from the valence band edge (or HOMO) to the conduction band edge (or LUMO) in the light absorber. The electron is then injected to the conduction band of the semiconductor and transports through the mesoporous network via diffusion to the front contact. This leaves the light absorber in an oxidized state and to reduce it, an electron from the HOMO of the hole conductor moves to the valence band edge (HOMO) of the light absorber. This creates a hole in the hole conductor, and for a solid molecular hole conductor, this hole is transported between the hole conducting molecules in a hopping manner until it reaches the back contact [63]. The key function, electron and

hole charge separation, in a mesoscopic solar cell thus happens at the interfaces of the different materials and the electrons and holes are transported through the oxide and the hole conductor respectively. The large surface area of the mesoporous semiconductor creates a large interface where charge separation can occur. TiO_2 is the most widely used semiconductor for mesoscopic solar cells due to its good semiconductor properties and ability to form stable nanoparticles and porous structures.

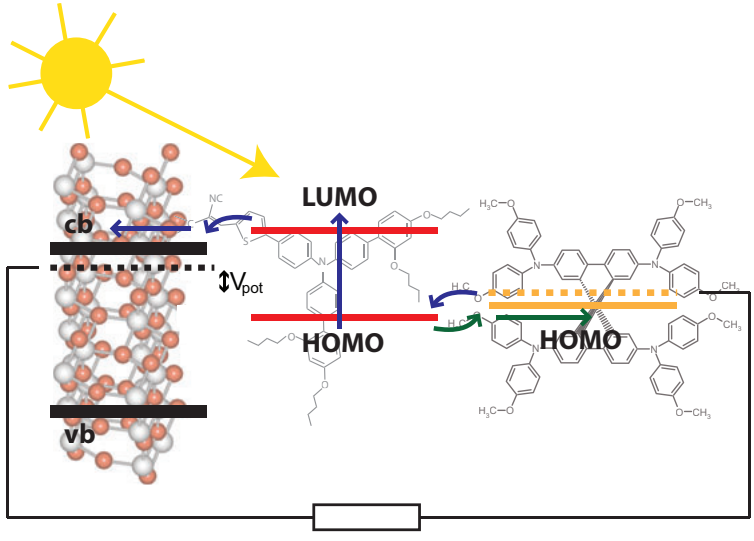

Figure 5.1. The working principle of a mesoscopic solar cell, in this case a solid state dye-sensitized solar cell, showing the most important energy levels in the semiconductor electrode (TiO_2), the dye molecule and the hole transporting material (HTM)

5.1.2 Energy levels and alignments

The energy levels in the different materials in the solar cell must be properly chosen and well aligned for a good working solar cell. The band gap in the light absorber should be sufficient for absorbing visible light. The conduction band edge in the light absorber must have slightly higher energy than the conduction band edge of the semiconductor, so that electron injection from the light absorber to the semiconductor is energetically favorable. The same holds for the HOMO in the hole conducting molecule relative the valence band edge in the light absorber. The output voltage of the solar cell is limited by the difference between the conduction band edge in the semiconductor and the HOMO in the hole conducting molecule (or rather the quasi-Fermi level of electrons in the semiconductor and the quasi-Fermi level for holes in the hole conductor). All these energy levels can be changed in various ways. By changing the semiconductor, the conduction band edge will change. Different light absorbers have

different band gaps and their position relative, for example, the conduction band edge in the semiconductor can differ. The HOMO in the hole conductor can also vary between different materials. Examples of light absorbers and hole conductors can be found in figure 5.2 where the molecular structure of all molecular materials used in this thesis is shown.

The energy levels can be measured with various methods, for example UV photoelectron spectroscopy (UPS), flat band potential and cyclic voltammetry, where one material at a time can be studied. The relative energy levels between two materials might however change at the interface when the materials are brought in contact with each other [26, 64, 65] as described in chapter 2.3. Therefore it is useful to study a complete interface, which can be achieved using XPS or HAXPES [51, 66].

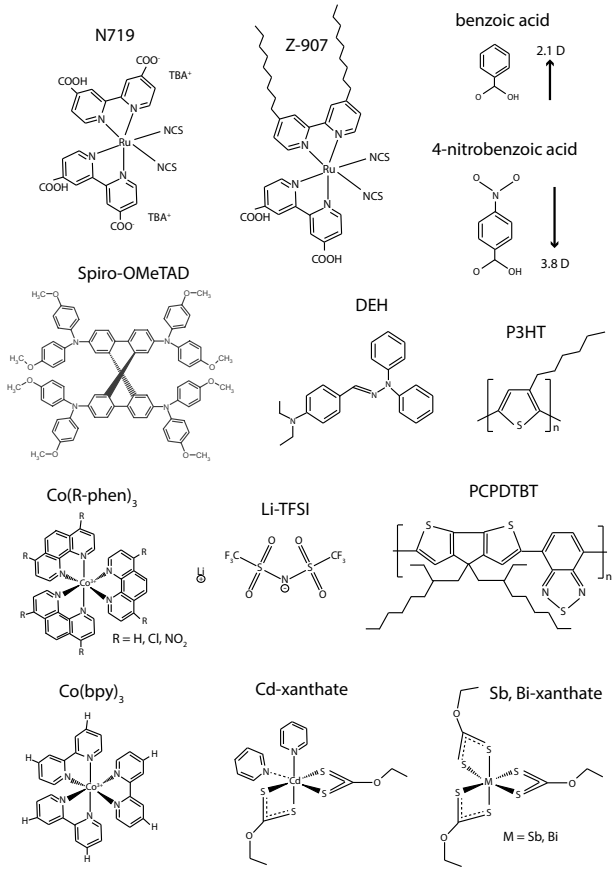

Figure 5.2. Structures of the molecular materials described in this thesis. N719 and Z-907 are dye molecules; Spiro-OMeTAD, DEH, P3HT and PCPDTBT are used as hole conductors; benzoic acid and 4-nitrobenzoic acid are dipole molecules; Li-TFSI, Co(R-phen) and Co(bpy) are used to modify the energy levels in hole conductors; Cd-xanthate, Sb-xanthate and Bi-xanthate are precursors that can be transformed to metal sulfides.

When a solar cell is not illuminated, charges will be redistributed between the different material interfaces as to equillibrate the Fermi level. During illumination, electrons are forced into the conduction band of the mesoporous semiconductor shifting the Fermi level of the semiconductor towards the conduction band. Similarly, the concentration of holes will increase in the hole conductor HOMO level shifting the Fermi level in this material towards the HOMO. When illuminated, the system is not in electrical equillibrium and the energy differences give rise to a photovoltage, which can be represented by different Fermi levels in different parts of the system.

The photoelectron spectroscopy measurements in this thesis are not performed on solar cells in operation, mainly since no complete solar cells are studied. Therefore the system can be regarded as being in the dark with a common Fermi level for materials in electric contact.

The main transport of charges in a mesoscopic solar cell take place in the mesoporous semiconductor (electrons) and the hole conductor (holes). Both these materials are semiconducting and their conductivity can be increased by doping, *i.e.* adding impurity levels in the band gap which shifts the Fermi level. These impurity levels are close to the conduction band for an n-doped material and close to the valence band for a p-doped material. From the impurity level, electrons and holes can be thermally excited to the conduction band and valence band respectively and both impurity and band levels can transport charges. The electrons and holes are however still taken out from the solar cell at the Fermi levels. Since photoelectron spectroscopy can probe all occupied levels it is in principle possible to measure the impurity levels, however, the amount of electrons in impurity levels can often be too small to be detected.

5.2 Basic solar cell characterization

To characterize solar cells, many different techniques are used giving information about the function in the different parts of the device. A few of the basic techniques will be described here: UV-vis shows the absorption characteristics; IV-measurements characterizes the overall energy conversion of the solar cell; IPCE gives information about which solar energies or wavelength that can contribute to the photocurrent. These techniques are illustrated below with results from this thesis.

A few other important techniques are also worth mentioning, even though they will not be treated in more detail. For example, to study the kinetics of the charge transfer processes in the solar cell in more detail, pump-probe techniques such as transient absorption spectroscopy [67] and photo-induced absorption spectroscopy [68] can be used. The transport time for the electrons in the solar cell and the electron lifetime in the mesoporous semiconductor can be studied with photocurrent and photovoltage measurements where the light is intensity modulated [7, 69].

5.2.1 UV-vis absorption

Light absorption is a key process in the solar cells. In measurements of the UV-vis absorption characteristics the sample is exposed to light where the wavelength is scanned (through a monochromator) from visible to near infrared. The ratio of light that is transmitted through the sample is measured with a detector for each wavelength and compared with that incident on the sample. The transmittance, T, can then be used to calculate the absorbance according to equation 5.1.

$$Absorbance = -log_{10}T \tag{5.1}$$

Figure 5.3(a) shows the absorbance in films of the hole conducting molecule spiro-OMeTAD mixed with varying amounts of Li-TFSI. The large peak at a wavelenght of 385 nm is absorption in the neutral spiro-OMeTAD molecule [70], while the smaller feature at 500 nm is from oxidized spiro-OMeTAD molecules [71]. Since the latter peak increases with addition of Li-TFSI and since the Li-TFSI does not absorb in the visible region, the effect of adding Li-TFSI is an oxidation of the spiro-OMeTAD film. This will be discussed further in chapter 5.4.2.

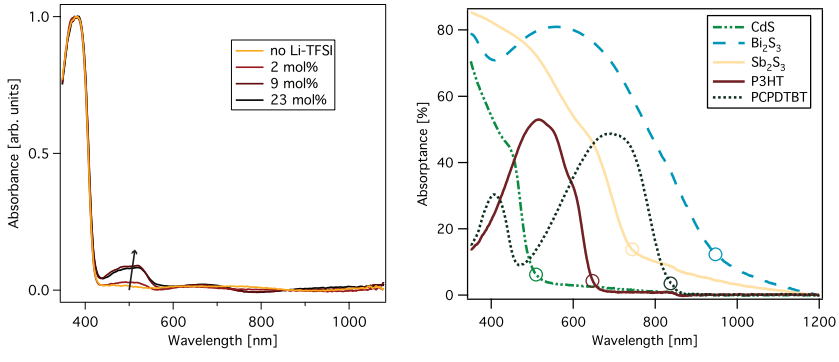

(a) (b)

Figure 5.3. (a) Absorbance in spiro-OMeTAD where the arrow indicate increasing concentration of Li-TFSI. (b) Absorption in three metal sulfides and two polymers.

If the samples are scattering a lot of light it can be necessary to use an integrating sphere to focus the transmitted light on the detector. In this case both the transmittance, T, and reflectance, R, can be measured and related to the absorption through equation 5.2.

$$Absorption = 1 - T - R \tag{5.2}$$

The absorption of three different metal sulfides and two polymers measured through an integrating sphere can be seen in figure 5.3(b). The circles mark the absorption onsets, which can be used to etimate the bandgap of the semiconducting metal sulfides.

Absorbance/absorption studies can be performed on solutions, sensitized electrodes or molecular films on conducting glass, but complete solar cell devices are not generally studied (since the counter electrode blocks the light).

5.2.2 IV-measurements

The energy conversion efficiency of a solar cell is deduced from an IV-curve, as in figure 5.4. The complete solar cell is illuminated with a lamp with a spectrum similar to the sun (AM1.5). During illumination, the current is measured as a function of the voltage, which is varied through a variable external load. The current at 0 V gives the short-circuit current (I_{sc}) and the voltage at 0 current is the open-circuit voltage (V_{oc}). As the power is the product of V and I, an optimal IV-curve is a square and the deviation from the theoretical maximum of the device is described by the fill factor (FF). The efficiency, η, is calculated as in equation 5.3

$$\eta = \frac{I_{sc}V_{oc}FF}{P_{in}} \tag{5.3}$$

where P_{in} is the light intensity.

The IV-curve in figure 5.4 and the extracted solar cell characteristics in table 5.1 describes dye-sensitized solar cells whith ZnO as mesoporous electrode. The electrodes are sensitized with the dye molecules N719 and Z-907 where in some cases water has been included in the sensitization process. It can be seen that water does not change the overall efficiency for Z-907, but for N719 the addition of water increases the efficiency 50 times, mainly by increasing the current. The reason for this enhancement with water will be discussed in chapter 5.3.1.1.

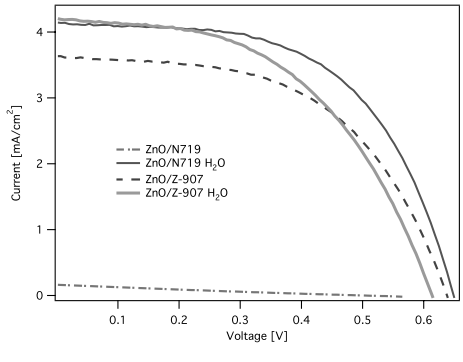

Figure 5.4. IV curve of ZnO dye-sensitized solar cells with two different dye molecules where in some cases water was added in the dye-sensitization process.

Table 5.1. *IV measurements of ZnO dye-sensitized solar cells showing the overall efficiency η, the open circuit voltage V_{oc}, the short circuit current I_{sc} and the fill factor FF.*

Cell	η [%]	V_{oc} [V]	I_{sc} [mA/cm^2]	FF
ZnO/N719	0.03	0.60	0.22	0.23
ZnO/N719 H_2O	1.5	0.65	4.15	0.57
ZnO/Z-907	1.3	0.64	3.64	0.54
ZnO/Z-907 H_2O	1.3	0.61	4.20	0.50

5.2.3 IPCE

Spectral information on the photon to current conversion in a solar cell can be obtained from IPCE measurements. IPCE is an abbreviation of Incident Photon to Current conversion Efficiency and measures the current generated at each wavelenght over the visible range. IPCE can also be called the external quantum efficiency (EQE). A monochromator selects the wavelenght of the light source and the current from the solar cell is measured as the wavelenght is scanned. The IPCE is calculated as the ratio of outgoing electrons and incoming photons as

$$IPCE = \frac{hc}{e}\frac{i_{ph}(\lambda)}{\lambda P(\lambda)} \tag{5.4}$$

where h, c and e are constants[1], i_{ph} is the photocurrent density, P is the light density and λ is the wavelength. If the charge generation in the solar cell is efficient, the IPCE spectrum should match the absorption spectrum.

In figure 5.5 two examples of IPCE spectra are given, where figure 5.5(a) illustrates the IPCE of solid state dye-sensitized solar cells with the dye D35 and the three different hole conductors spiro-OMeTAD, P3HT and DEH. Figure 5.5(b) shows IPCE measurements of semiconductor sensitized solar cells whith the light absorbers CdS, Sb_2S_3 or Bi_2S_3 and P3HT or PCPDTBT as hole conductor. For Bi_2S_3 the highest IPCE is observed for wavelengths corresponding to absorption in P3HT rather than the metal sulfide (compare with figure 5.3(b)). From this it can be concluded that Bi_2S_3 does not contribute to the photocurrent in the device (which will be discussed more in chapter 5.3.2.1).

5.3 Light absorbers

Mesoscopic solar cells are very often categorized by the light absorber used in the device since this is the heart of the conversion of light to electricity, *i.e.* light absorption and charge separation. A large variety of dye molecules and small band-gap semiconductors are used in different solar cell configurations and in

[1]Where h is Planck's constant, c is the speed of light and e is the elementary charge.

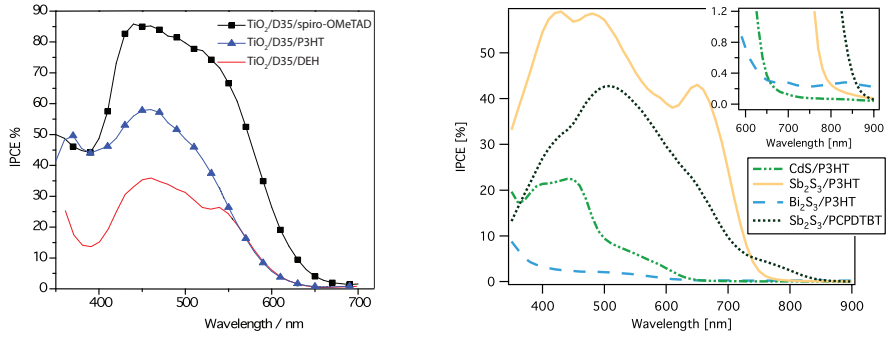

(a) (b)

Figure 5.5. (a) IPCE of solid state dye-sensitized solar cells based on the different hole conducting molecules spiro-OMeTAD, P3HT [72] and DEH [73]. (b) IPCE of semiconductor sensitized solar cells whith the light absorbers CdS, Sb_2S_3 or Bi_2S_3 and the hole conductors P3HT and PCPDTBT.

this section I will touch upon a few of these. The discussion is divided into the type of device characterized by the light absorber: Ru-complexes are discussed as dye molecules in dye-sensitized solar cells; metal sulfides are treated in terms of semiconductor-sensitized solar cells; perovskite materials are discussed as light absorbers in perovskite solar cells. Each section starts with a general description about the respective solar cell configuration, followed by the important experimental results, for the particular light absorber, obtained in this thesis.

5.3.1 Dye-sensitized solar cells

Dye-sensitized solar cells were the first emerging mesoscopic solar cells after O'Regan and Grätzel published their results on a solar cell with TiO_2 nanoparticles, a Ru-complex as light absorber and a iodide/triiodide redox electrolyte [5]. For a long time different Ru-complexes were the most widely used dye molecules [10], but more recently, organic molecules are becoming a more and more promising alternative [74, 75]. Organic dyes typically have a high extinction coefficient (which is absorption per unit area for the adsorbed molecule). This is useful for solid state dye-sensitized solar cells since a bad pore filling of the hole conductors in the TiO_2 film and poor conductivity in the hole conducting material reduces the optimal film thickness and therefore the amount of dye molecules [75, 76]. Dye molecules are typically adsorbed to the mesoporous semiconductor surface by putting the semiconductor electrode in a solution containing the dye molecules. A molecule that is adsorbed to the TiO_2 surface together with the dye-molecule, a so called co-adsorber, can increase the efficiency of the solar cell [77].

For many years, electrolytes including I^-/I^{3-} redox couples, were the standard choice for regeneration of the dye molecules in dye-sensitized solar cells. The regeneration process is however complex and a large driving force is needed to regenerate the dye (*i.e.*, a large distance between the redox potential of the electrolyte and the HOMO of the dye). This reduces the V_{oc} in the solar cell [78]. A few years ago a Co^{2+}/Co^{3+} redox couple was sucessfully incoorporated together with an organic dye [20, 79]. In contrast to I^-/I^{3-} where two electrons are involved in the redox process, the Co^{2+}/Co^{3+} redox reaction includes only one electron and does not need as large driving force for regeneration. A liquid electrolyte requires a good encapsulation of the solar cell, where the front and back contact are sealed together. Both the front and back contact in a liquid dye-sensitized device are typically conducting glass.

5.3.1.1 The influence of water on semiconductor/dye interfaces

How water can affect the dye adsorption to the surface as well as the solar cell performance of dye-sensitized mesoporous ZnO or TiO_2 is the topic of paper **I** and **II**. For the studies of ZnO solar cells, water was included in the dye solutions of the dyes N719 and Z-907, during sensitization. For photoelectron spectrosocpy studies, two different sensitization times were used, 10 min and 15 h. For the studies on TiO_2, the sensitized electrodes were exposed to water after a sensitization for 12 h using the same dyes. In all cases, the results were compared to samples that had not been exposed to water. The ZnO and TiO_2 were thus exposed to water in different steps of the sample preparation, but the results show similarities. Solar cells were also assemblied with the mesoporous electrode sensitized as described above, and with a liquid electrolyte containing I^-/I^{3-} redox couples.

The dyes N719 and Z-907 are both metal complexes with Ru as the center atom and with bipyridyl ligands. The main structural difference is that N719 is deprotonated and therefore includes the counter ion TBA^+, while Z-907 has long alkyl chains making this dye hydrofobic.

The performance of ZnO solar cells with and without water in the sensitization process are described in figure 5.4 and table 5.1. As can be seen, the performance of solar cells including the dye N719 increases greatly when including water in the dye solution. For Z-907, there is not much difference when water is included or not. For solar cells based on TiO_2, the behavour is similar for the Z-907 dye for which solar cells are not affected much by water. For N719 there is on the other hand a decrease in solar cell efficiency from 2.1 to 1.5 % when exposed to water.

Changes in the amount of dye molecules adsorbed to the semiconducting surface can be determined by comparing the intensity of a core level originating from the dye, with a core level from the substrate. Such comparison is found in table 5.2 where the intensity of the Ru $3d_{5/2}$ core level peak is compared to Zn 3p or Ti $2p_{3/2}$ depending on the substrate. Note that the different photoionization cross sections for the different core levels are not taken into

accout in the ratios in table 5.2, therefore should the Ru/Zn ratios not be compared with the Ru/Ti ratios directly. A comparison between samples exposed to water or not for a given semiconducor is however still valid.

Table 5.2. *Ratios between Ru $3d_{5/2}$ and Zn 3p intensities for ZnO samples and ratios between Ru $3d_{5/2}$ and Ti $2p_{3/2}$ for TiO_2 samples measured with a photon energy of 758 eV. A sensitization time of 15 h was used for ZnO and 12 h for TiO_2.*

Ratio	Sample	no H_2O	H_2O
Ru/Zn	ZnO/N719	1.72	0.19
	ZnO/Z-907	0.13	0.15
Ru/Ti	TiO_2/N719	6.6	3.6
	TiO_2/Z-907	8.1	8.4

If starting with the dye Z-907, a similar behaviour is found on both substrates where the ratio increases slightly when the samples are exposed to water. This implies that more dye molecules adsorbs to the surface when water is included in the process, which could be a consequence from Z-907 not being soluble in water. For N719 the amount of dye decreases when the samples are exposed to water, but the extent differs for the two substrates. For TiO_2/N719, the decreased ratio is interpreted as dye desorption, which agrees with the decreased solar cell efficiency for solar cells exposed to water. For ZnO/N719 the interpretation is different since the ratio with water is more similar to the ratios found for Z-907. For this sample it is the ratio without water that stands out, being ten times higher than the other ratios for the ZnO samples. The high Ru/Zn ratio for the ZnO/N719 sample without water could indicate a multilayer formation or that the dye molecules form aggregates with Zn^{2+} ions. Earlier studies have shown that ZnO can dissolve in an acidic environment forming Zn^{2+} [80]. This together with the fact that the Zn 3p core level is visible despite the large amount of dye molecules, indicates aggregation rather than a pure multilayer formation. For the shorter sensitization time of 10 min, the amounts are comparable for all ZnO samples (the ratios are approximately 0.1), and therefore these samples are used in the following characterization of the bonding behaviour.

If the differences in photoionization cross sections, the analyzer transmission and the substrate element density is taken into account, it was found that the packing of the dye molecules are similar for TiO_2/N719 and ZnO/N719 samples if aggregation is avoided in the latter case.

Water-induced changes of the bonding of the adsorbed dye molecules on the ZnO and TiO_2 substrates can be followed by the S 2p core level, as shown in figure 5.6. S 2p has a spin-orbit split of 1.18 eV where the intensity ratio is 1:2 between the S $2p_{1/2}$ and the S $2p_{3/2}$ levels. In all spectra in figure 5.6, the S 2p is composed of two spin-orbit doublets. In a multilayer of N719 there is only one spin-orbit doublet [81], and the second peak doublet at higher binding energy appears after adsorption to the semiconductor surface. The relative

intensities of the two spin-orbit doublets indicate different interactions with the surface and/or other dye molecules. For TiO_2/Z-907 and ZnO/Z-907, there is no change in the relative ratios of the S 2p components when exposing the sample to water. The total intensity of S 2p increases with water, which can be related to the slightly larger amounts of dye molecules on the surface. For N719 there is a larger difference when water is used or not. In the TiO_2/N719 sample, the high binding energy peak increases from 10 to 31% of the total peak area when including water. For ZnO/N719 the increase is from 34 to 56%. This indicates that the N719 dye molecules binds differently to the surface when exposed to water. The larger amount of the high binding energy contribution to the S 2p core level in ZnO samples also indicates that the molecules bind differently to ZnO compared to TiO_2.

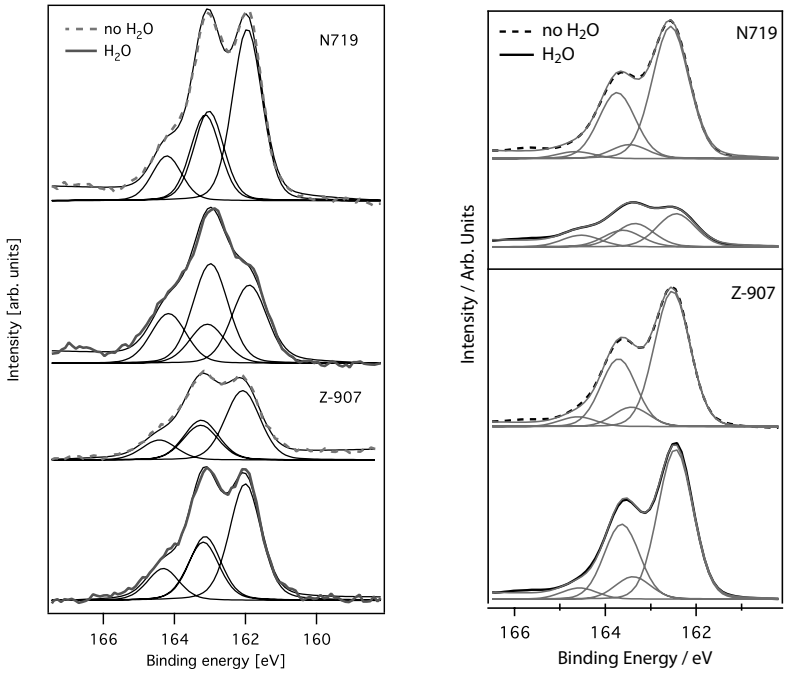

Figure 5.6. The S 2p core level measured with a photon energy of 454 eV for N719 and Z-907 on ZnO (a) and TiO_2 (b). The spectra are intensity calibrated using the Ru $3d_{5/2}$ level.

In summary, the hydrfobic chains in the Z-907 dye protect the dye from changes when exposing the solar cell to water. For N719, the amount of dye on the semiconducting surface decreases with water and the binding to the surface changes. For TiO_2/N719 the lower amount of dye molecules results in lower solar cell performance. For ZnO/N719 on the other hand, the solar cell

performance increases largely, explained by reducing dye aggregation at the surface.

5.3.2 Semiconductor-sensitized solar cells

In a semiconductor-sensitized solar cell, a thin film of a small bandgap semiconductor act as light absorber. To use a semiconductor instead of a dye offers some advantages including a simple solution-based preparation and the possibility to modify the band gap by quantum confinement effects in small particles of the semiconductor (quantum dots) [82]. If using the light absorber together with a solid hole conducting material, the device is also called an ETA cell (extremely thin absorber).

Examples of solution-processable nanocrystalline metal chalcogenides used as light absorbers in semiconductor-sensitized solar cells are metal sulfides such as Sb_2S_3, CdS and PbS and the metal selenides Sb_2Se_3, CdSe and PbSe [11]. Similar materials are also used as buffer layers in thin film solar cells [83]. The starting point for making these kinds of materials are precursors including the metal and the sulphur. In this work, a single molecular precursor including both the metal and the halide was used. This type of precursor is usually deposited into the mesoporous network from solution using spin-coating (a method also used for solid hole conducting materials). After spin-coating, the electrode is heated to 150–300° C during which the metal chalcogenide is formed. As briefely stated above, an understanding of interfacial structures and specifically of the energy alignment is important for improved understanding of such devices.

5.3.2.1 Energy level alignment in TiO_2/metal sulfide/polymer interfaces

Samples of mesoporous TiO_2 sensitized with the three different metal sulfides CdS, Sb_2S_3 or Bi_2S_3 and two different polymers P3HT or PCPDTBT were studied with photoelectron spectroscopy with soft X-rays (in paper **III**). The low photon energy was selected to be able to measure the outermost valence levels of the polymers, which are mainly consisting of carbon orbitals. CdS and Sb_2S_3 have successfully been used as light absorbers in semiconductor-sensitized solar cells, however, Bi_2S_3 has not. One goal with this study was to figure out why, by determining the energy level alignment between TiO_2, the sulfides and the polymers, the latter used as hole conductors in devices.

The valence levels of TiO_2 and TiO_2/metal sulfides can be found in figure 5.7(a). The TiO_2 substrate contributes to the spectra at binding energies between 3.2–8 eV. The outermost levels of the metal sulfides are found below 3.2 eV, where the orbital character is a mix between S 3p and metal s or p orbitals. The differences of the valence band edges between the TiO_2 and the metal sulfides can be estimated from the onsets of the outermost regions, see the inset to figure 5.7(a), and are 1.2 eV for CdS, 1.8 eV for Sb_2S_3 and 1.9 eV

for Bi_2S_3. The energy level alignments are illustrated in figure 5.8, where the optical band gaps are used to draw the conduction band edges.

After depositing a polymer on top of mesoporous TiO_2 sensitized with Sb_2S_3, the valence level spectra looks like in figure 5.7. The different shape of the spectra with the two polymers comes solely from a different thickness of the polymer over-standing layer where the P3HT film was thicker than the PCPDTBT film. A close-up of the valence band edges can be seen in the inset figure and reveals a difference of 0.4 eV between the edges in Sb_2S_3 and the polymers.

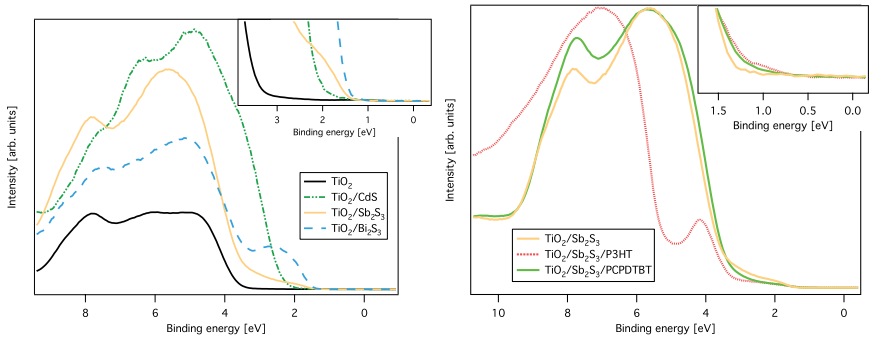

(a) (b)

Figure 5.7. The valence levels of TiO_2 and TiO_2/metal sulfides (a) and TiO_2/Sb_2S_3/polymer samples (b) measured with a photon energy of 150 eV. The highest peaks are scaled to show the same height in the spectra in (b). In (a) the intensities are normalized using the Ti 3p core level. The inset shows a closeup of the outermost region where the circles mark the estimated valence band edges.

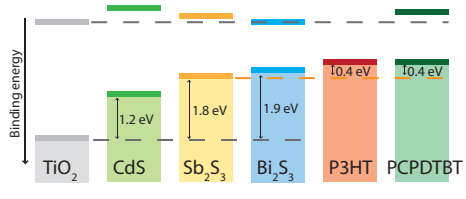

Figure 5.8. The energy level alignment of TiO_2, metal sulfides and polymers. The arrows indicates the measured distances between the valence band edges. Band gaps are estimated from the absorption measurements for metal sulfides and polymers, for TiO_2, the common value 3.2 eV is used for the band gap [84].

To have a sufficient driving force for electron injection from the excited metal sulfide to the TiO_2 there must be a certain distance between the conduction band edges of the two materials. The same holds for the HOMO of the polymer and the valence band edge of the metal sulfide, so that there is a driving force for regeneration of the oxidized metal sulfide. The measured energy level alignment can therefore be used to predict, or understand, the

function of a device. Solar cells with the architecture TiO_2 (blocking layer)/ TiO_2 (mesoporous) /metal sulfide/P3HT/Ag were therefore built and the solar cell performance was compared to the measured energy level alignment.

The efficiency of solar cells with the different metal sulfides as light absorbers were 0.46% for CdS, 3.35% for Sb_2S_3 and 0.02% for Bi_2S_3. If comparing the IPCE spectra in figure 5.5(b) with the absorption spectra in figure 5.3(b) it is possible to predict where the short-circuit current is generated in the device. For CdS, the highest IPCE is found for absorption in the cadmium sulfide, however there is also some current that is generated in P3HT. The current is also limited by the large band gap in the CdS. Sb_2S_3 absorbs well up to a wavelenght of 740 eV and the corresponding IPCE is found in the same wavelength region. For Bi_2S_3 the picture is somewhat different since the highest IPCE is found in the wavelenght region where P3HT absorbs and the bismuth sulfide contributes very little to the current.

The low efficiency of the devices including Bi_2S_3 can be explained by the energy level alignment where it can be seen that Bi_2S_3 has no driving force for injecting electrons to the TiO_2 conduction band. Sb_2S_3 shows the most favourable energy level alignment and therefore also the best performing devices. Solar cells with CdS has a performance between the other two despite large driving force for both electron injection and regeneration, but the large band gap in CdS limits the generated current.

The results above show that photoelectron spectroscopy is very useful for a direct measurement of the energy level alignment of complete interfaces found in solar cell devices, as well as understanding the electronic structure and the materials chemistry. Such measurements can be used to predict electronic and chemical differences on an atomic level between materials, and therefore to better understand the function of devices.

5.3.3 Perovskite solar cells

Solution processable inorganic-organic perovskite materials has recently showed great usage as light-absorbers in mesoscopic solar cells and the perovskite solar cell is seen by many people as the new emerging solar cell [8, 15]. The perovskite material show a great deal of variety and can be used as light absorber, hole conductor, combined light absorber and electron conductor or as a combined light absorber and hole conductor.

A perovskite refer to a material with the general crystal structure ABX_3. Many different kinds of perovskite exist with diverse properties and a wide range of usage. The semiconducting perovskite structures, with a small band gap, that has successfully been incorporated in mesoscopic solar cells typically have the chemical structure $CH_3NH_3MX_3$ where M can be Pb or Sn and X is I, Br or Cl (or a mixture of these elements) [85–87]. The perovskite material can be made by mixing a CH_3NH_3X compound with MX_3 and heating this

mixture to 100° C. Even though the perovskite film is very thin (in the order of 5 nm), it shows crystalline behaviour.

Devices including perovskites benefit from using a solid hole conductor, since they are soluble in water and a liquid electrolyte can dissolve the perovskite [86]. Attempts to make a perovskite-sensitized solar cell with a liquid electrolyte resulted in lower efficiency and less stable devices, compared to when a solid hole conductor is used [88, 89]. Perovskites are also sensitive to moisture and special attention needs to be adressed to handle them. For this reason, all perovskite samples studied in this work were stored in argon between preparation and measurements.

5.3.3.1 The TiO_2/Perovskite interface

The $CH_3NH_3PbI_3$ perovskite was in a study (paper **IV**) deposited onto mesoporous TiO_2 in two different ways: a one-step technique where CH_3NH_3I and PbI_2 were mixed in solution and then spin-coated onto TiO_2; a two-step technique where first a solution of PbI_2 was spin-coated onto TiO_2 and then the electrode was dipped in a solution containing CH_3NH_3I. Both deposition techniques has shown to give very similar perovskite structures as indicated by similar core level binding energies and relative core level intensities. An estimation of the stoichiometry suggests that the expected perovskite material was formed for both synthesis routes (*i.e.* one- or two-step). The humidity during preparation of the perovskites was however shown to be important for the resulting structure. Two-step $CH_3NH_3PbI_3$ prepared under more humid conditions showed a Pb core level shift of 0.4 eV towards lower binding energy, and a stoichiometry far from the expected one (indicating excess units of CH_3NH_3I).

The valence levels of TiO_2, TiO_2/PbI_2 and $TiO_2/CH_3NH_3PbI_3$ deposited in one and two steps and measured with HAXPES are shown in figure 5.9, where TiO_2/PbI_2 is the first step in the two-step process. The two differently prepared perovskites show very similar valence levels, also very similar to the TiO_2/PbI_2 sample. This indicates that the valence levels in the perovskites to a large extent consists of the I and Pb orbitals. This result was also confirmed with DFT calculations. The valence band edge of TiO_2 is found at a higher binding energy compared to both TiO_2/PbI_2 and $TiO_2/CH_3NH_3PbI_3$ samples. The binding energy difference between the valence band edges of TiO_2 and TiO_2/PbI_2 is 1.75 eV, while it is 2.1 eV for the $TiO_2/CH_3NH_3PbI_3$ samples, as illustrated to the right in figure 5.9. The position of the valence band edge of the $CH_3NH_3PbI_3$ perovskite determined by HAXPES was recently confirmed by UPS [90].

5.3.3.2 The perovskite electronic structure

The $CH_3NH_3PbI_3$ perovskite material was studied in paper **IV** and in paper **V** this material was compared to the perovskite $CH_3NH_3PbBr_3$. In both materials, a small contribution from metallic lead was observed. This can be seen

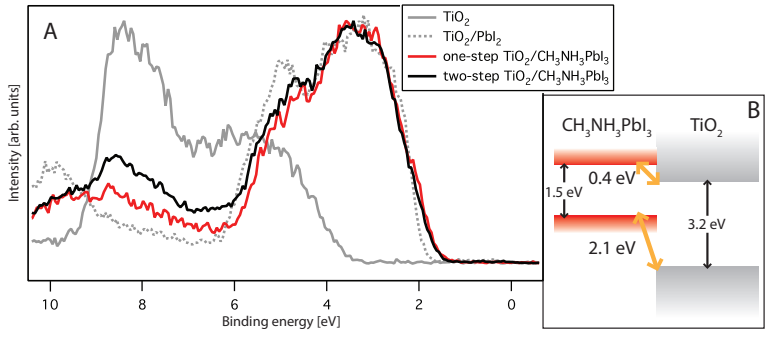

Figure 5.9. A. Valence levels of TiO_2, TiO_2/PbI_2 and $TiO_2/CH_3NH_3PbI_3$ processed in one and two steps measured with a photon energy of 4000 eV. B. A drawing of the energy level alignment where the optical band gaps are used.

in the Pb 4f spectra in figure 5.10(a), where peak doublets with lower intensity are observed at lower binding energy compared to the main peaks, and the smaller contributions are assigned to metallic lead. The metallic contribution to the lead core level in $CH_3NH_3PbI_3$ was modelled with DFT as a removal of two iodine atoms surrounding a lead atom. The calculated chemical shift (1 eV) is smaller than the experimental shift (1.6 eV), indicating that there can be many metallic lead atoms forming a cluster. Figure 5.10(a) also displays a different binding energy of the main Pb 4f core level doublet when comparing the two perovskites. The higher binding energy seen for the $CH_3NH_3PbBr_3$ perovskite could be explained by a charge analysis where a higher charge on the Pb atom was found in this perovskite.

The perovskite material can be well modelled with DFT calculations as demonstrated by figure 5.10(b). The top part of this figure shows the experimentally measured valence levels of the two perovskites $CH_3NH_3PbI_3$ and $CH_3NH_3PbBr_3$. A binding energy shift of the outermost valence levels when comparing the two perovskites is clearly observed. The $CH_3NH_3PbBr_3$ perovskite shows a higher binding energy of both the valence band edge and the most intense part of the valence levels. This binding energy shift is also seen in the total DOS and the I/Br PDOS in the calculated spectra. Both the outermost valence regions and also the binding energy region 6–18 eV is well described by the calculated Pb and I/Br contributions. The remaining part of the total DOS, the $CH_3NH_3^+$ ion, is, on the other hand, not represented by the experimental spectra. This is partly due to the high photon energy used in the measurements, which gives a higher cross section to the inorganic compounds.

5.4 Hole conducting materials

Organic solid hole conducting materials are used in solid state dye-sensitized, semiconductor-sensitized and perovskite solar cells. Problems of poor sta-

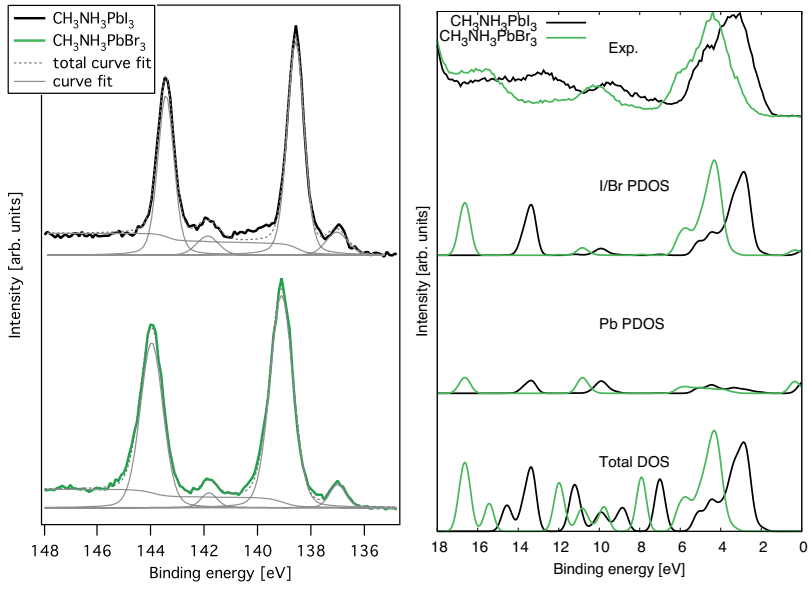

Figure 5.10. (a) The Pb4f core level for the two perovskites measured with a photon energy of 4000 eV. (b) Experimentally measured valence levels (top) together with the calculated total density of states (DOS) and the Pb, I and Br partial density of states (PDOS).

bility related to encapsulation of the electrolyte in the liquid device was one of the starting points for developing the solid state devices [10, 21]. In perovskite solar cells, a solid hole conducting material is almost obligatory since a liquid electrolyte could dissolve the perovskite light absorber. Studies of the hole conductor itself is therefore of interest for a large part of the mesoscopic solar cell community. A large variety of solid hole conducting materials are studied, both inorganic and organic, *e.g.* the inorganic material CuSCN [9], the polymers P3HT [91] and PEDOT [92], or different kind of molecules [10, 21, 73, 93, 94]. A triphenylamine based molecule called spiro-OMeTAD is to this date the most widely used hole conducting material. In this thesis, different aspects of modifying the energy levels of the hole conductors P3HT, DEH and spiro-OMeTAD are treated (for molecular structures, see figure 5.2).

Many of the organic hole conductor materials suffers however from low hole mobility, and low conductivity, which is often increased by doping of the material. The hole conductor is often incorporated into the porous semiconductor network from solution by spin-coating. With this method molecules may have problems to infiltrate efficiently into the deeper pores. For this reason, alternative ways to infiltrate the hole conductors are of interest. One way is by melting the hole conductor and infiltrate it in its liquid form [73]. This method was successfully used to produce a working solar cell using DEH as hole con-

ductor material. Another drawback with many solid hole conducting materials is a risk of short-circuiting between the hole conductor and the front contact. To avoid this, a dense TiO_2 layer is deposited onto the conducting glass, before the deposition of the mesoporous TiO_2 [95].

Different additives are often used to fine tune the properties of the different materials and interfaces in the solar cell. One element that can shift the energy levels is lithium. Li^+ ions has been showed to move the conduction band of TiO_2 downwards and also to increases the conductivity of spiro-OMeTAD[10, 96, 97]. Another additive, 4-tert butylpyridine (tBP), moves the conduction band edge of TiO_2 upwards and reduces recombination in the solar cell [97]. The energetics at interfaces can also be changed by adding small dipole molecule at the interface.

An example of the performance of solid state dye-sensitized solar cells containing the three different hole conductors spiro-OMeTAD, P3HT and DEH can be seen in figure 5.5(a) where the incident photon to current conversion efficiency (IPCE) is plotted as a function of the wavelength. The same semiconductor material (TiO_2) and dye molecule (D35) were used in all three cases. The IPCE shows that all these molecules work as a hole conducting material in a solid state dye-sensitized solar cell. Spiro-OMeTAD gives in comparison the highest maximum IPCE of 85%, while this number for P3HT and DEH is 60% and 35% respectively [72, 73].

The hole conducting molecules, spiro-OMeTAD[2] and DEH[3] and the polymer P3HT[4] used in the following discussion were spin coated from solution onto conducting glass or onto TiO_2 electrodes. The TiO_2 surface was also modified with dipole molecules[5] that had been adsorbed to the surface by putting the TiO_2 film in a solution containing the dipole molecules. When applicable, a Li-salt[6] or different Co(+III) complexes were added to the hole conductor solution before spin coating. All samples were made *ex-situ* and transferred into the vacuum chambers from air. Below different holeconductors are compared and the effects from additives are discussed based on photoelectron spectroscopy measurements.

5.4.1 Energy level alignment due to interfacial modification

The energy levels in a fully assembled TiO_2/dipole molecule/P3HT interface was investigated using HAXPES in paper **VI**. Two different dipole molecules, 4-nitrobenzoic acid and benzoic acid, with dipole moments in different directions (3.8 D and -2.1 D respectively [98]) were adsorbed onto TiO_2 electrodes. The polymer P3HT was then spin-coated on top of the electrodes. Changes in

[2] 2,2'7,7'-tetrakis (N,N'-di-p-methoxyphenyl-amine)-9,9'-spiro-bifluorene
[3] 4-(diethylamino)benzaldehyde-1,1)-diphenyl-hydrazone
[4] poly(3-hexylthiophene)
[5] 4-nitrobenzoic acid and benzoic acid
[6] lithium bistrifluoromethylsulfonylamine

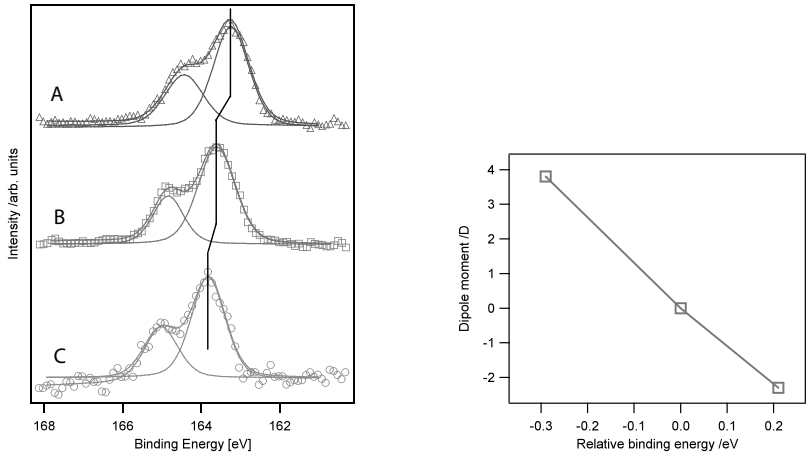

(a) (b)

Figure 5.11. (a) The sulphur S 2p core level measured with a photon energy of 2010 eV for TiO_2/P3HT interfaces including (A) 4-nitrobenzoic acid, (B) no dipole molecule and (C) benzoic acid. (b) The relative binding energy of the S 2p level versus the dipole moment.

energy level alignment were followed by measuring the core levels from the bulk TiO_2 and the bulk P3HT.

One element that is found in the polymer, but not in the dipole molecules, nor in the substrate is sulphur. Similarly, the element titanium is only found in the inorganic substrate. By comparing the binding energy of sulphur from the polymer with that of titanium from the substrate, it is possible to study the effect of the dipole molecules on the interfacial energy level alignment. In figure 5.11(a), the S 2p signal is shown and the binding energy is referenced versus the Ti 2p signal. It is seen that when using 4-nitrobenzoic acid the S 2p signal is shifted towards lower binding energies compared to when no dipole molecule is used. The S 2p signal from the sample including benzoic acid is shifted towards higher binding energy. The shifts in different directions corresponds well with the different signs of the dipole moments. Figure 5.11(b) shows the binding energy shift of S 2p versus Ti 2p as a function of the dipole moment. The relation has linear behavior, showing that a larger dipole moment gives a larger energy level shift.

A common model for describing the energy level shift caused be dipole molecules placed between two other materials is found in figure 5.12. When the dipole molecule has a negative charge towards the TiO_2 and a positive charge towards the polymer, the energy levels in the polymer shifts to higher binding energies, as is the case for benzoic acid. With the dipole moment in the other direction, the energy levels in the polymer is shifted towards lower

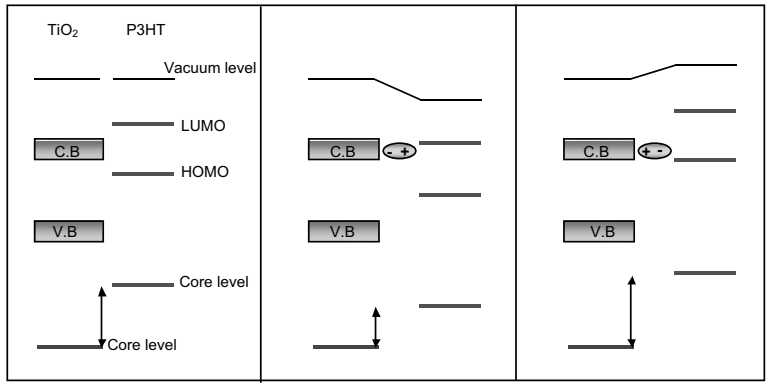

Figure 5.12. Selected energy levels in a TiO_2/polymer interface with (middle and right) and without (left) a dipole molecule in between.

binding energies, as for 4-nitrobenzoic acid. The model describes well the behavior of interfaces with dipole molecules.

5.4.2 Energy level shifts due to additives

Three different hole conducting molecules spiro-OMeTAD (in paper **VII**), DEH and P3HT (in paper **VIII**), have been mixed with the salt Li-TFSI and the effect on the energy levels in the mixture have been studied using HAXPES. Different concentrations of the salt have been used to quantitatively follow the effect.

Figure 5.13 shows measurements of the carbon C 1s level of the spiro-OMeTAD, DEH and P3HT molecules with different amounts of Li-TFSI. For spiro-OMeTAD, measurements using the photon energies 2010 and 6030 eV were very similar and the measurements with a photon energy of 2010 eV are shown here. For DEH, the studied effect of adding Li-TFSI was more clear in the bulk sensitive spectra measured with a photon energy of 6030 eV. For P3HT a photon energy of 4000 eV was used. For all hole conducting molecules, the broad peak centered around 285 eV comes from all the carbon atoms in the hole conductors. The smaller peak at 293 eV seen in the C 1s spectra of spiro-OMeTAD and DEH is from the carbon atoms in the TFSI molecule. It can be seen in figure 5.13 that the latter peak increases with higher concentration of Li-TFSI in spiro-OMeTAD and DEH. In P3HT, a peak indicating the precence of Li-TFSI can not be observed.

All spectra are binding energy calibrated versus the Fermi level (set to zero binding energy) and as can be seen in figure 5.13(a), Li-TFSI causes the large peak centered at 285 eV to shift 0.8 eV towards lower binding energies for spiro-OMeTAD. For DEH and P3HT similar shifts are seen when adding Li-TFSI and the shifts are in these cases up to 0.4 eV and 0.6 eV respectively, see

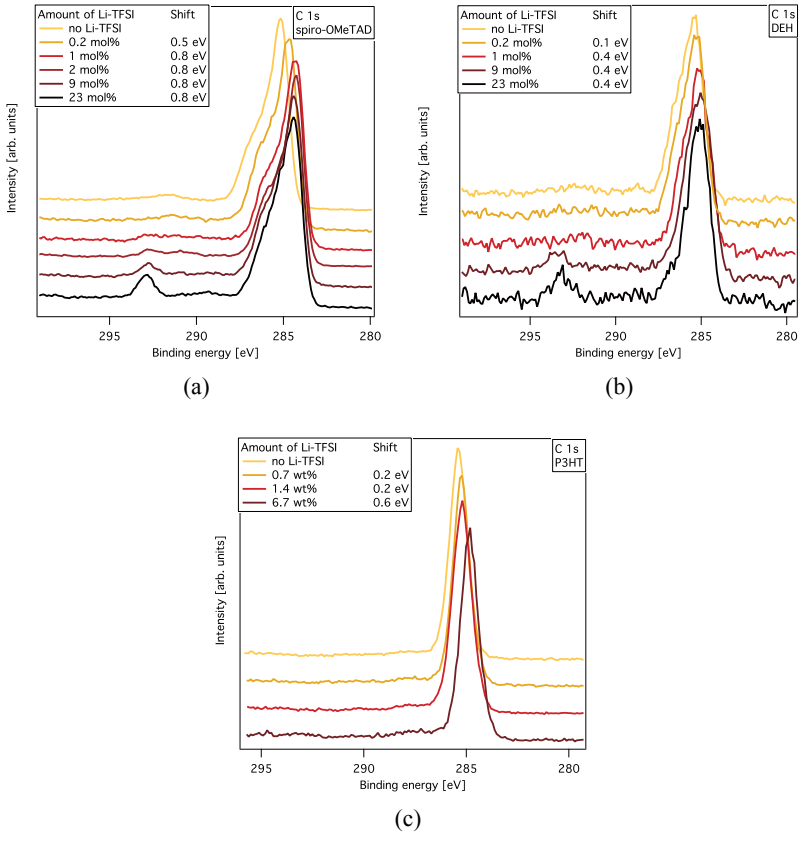

Figure 5.13. The C 1s core level of spiro-OMeTAD measured with a photon energy of 2010 eV (a), DEH measured with a photon energy of 6030 eV (b) and P3HT measured with a photon energy of 4000 eV (c). Different amounts of Li-TFSI was added to the hole conducting materials.

figures 5.13(b) and 5.13(c). The shifts are explained by a shift of the Fermi level towards the highest occupied levels in the molecule.

A Fermi level shift towards the valence levels is for semiconductors considered as a p-doping of the material (see for example chapter 2). The effect of adding Li-TFSI is hence the same as if spiro-OMeTAD, DEH and P3HT had been p-doped. This is illustrated in figure 5.14. These results agrees well with the earlier findings that Li-TFSI increases the conductivity of spiro-OMeTAD [99] which can be one reason for the increased solar cell efficiency when using this additive. The modified energy levels can also be more energetically favorable for the functioning of the dye-sensitized solar cell and thereby enhance the overall efficiency. However this Li-salt does not affect all hole conductors in the same way, observed here as different magnitudes of the Fermi level shifts for spiro-OMeTAD, DEH and P3HT respectively.

An explanation that Li-TFSI can act as a p-dopant despite itself not being redox active is that it causes a reaction with oxygen. In this reaction, Li_xO_y can be formed which is the real cause of the doping [100].

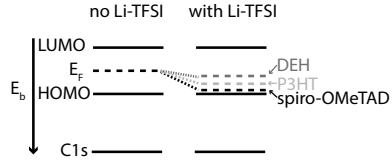

Figure 5.14. Selected energy levels in spiro-OMeTAD, DEH or P3HT with and without the addition of Li-TFSI showing the energy level shifts.

5.4.3 Controlled doping of spiro-OMeTAD

Doping of a molecular hole conducting material can also be performed in a more controlled way with a redox active dopant. A slightly different redox potential of the dopant compared to the hole conducting molecule induces a charge transfer, resulting in a modified Fermi level and increased conductivity. A Co(+III) complex enhances for example the electronic properties in spiro-OMeTAD, which then show great promise as hole conducting material in various kinds of mesoscopic solar cells [21, 86, 87, 101].

In paper **VIII**, we study the effect of doping spiro-OMeTAD with Co(+III) complexes with varying redox potentials [102]. The C 1s core levels of pure spiro-OMeTAD together with spiro-OMeTAD mixed with different Co(+III) complexes are displayed in figure 5.15(a). All core levels are normalized to the highest peak and for pure spiro-OMeTAD the main peak is centered around a binding energy of 285 eV. When adding $[Co(bpy)_3]^{3+}$, the peak remains at similar binding energy but when adding the other Co(+III) complexes, there is a shift of the C 1s level towards lower binding energy. The N 1s core level shifts in a similar manner and in figure 5.15(b) the shifts are plotted as a function of the redox potential of the Co(+III) complex. The vertical line indicates the first oxidation potential of undoped spiro-OMeTAD [21] and the error bars indicates small binding energy differences between the C 1s and N 1s core levels. It can be seen that the more positive redox potential of the Co(+III) complex, the larger is the chemical shift in spiro-OMeTAD. Similar to when Li-TFSI was added to spiro-OMeTAD, this core level shift indicates a shift of the Fermi level towards the HOMO in the hole-conductor, which equals p-doping.

5.4.4 Depth profiling of the mixed systems

As described in chapter 3.7 the depth sensitivity of the measurements can be changed by varying the photon energy. A lower photon energy gives surface

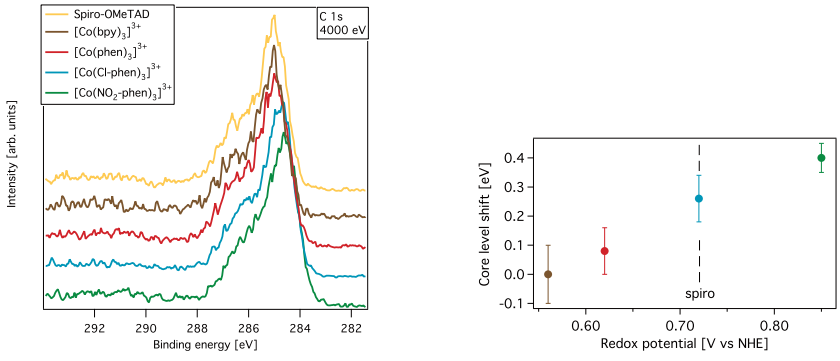

(a) (b)

Figure 5.15. (a) The C 1s core level of spiro-OMeTAD doped with Co(+III) complexes with varying redox potential and measured with a photon energy of 4000 eV. (b) The core level shift of the C 1s and N 1s core levels plotted as a function of the redox potential of the Co(+III) complex.

sensitive measurements while a higher photon energy gives more bulk sensitive measurements. In the experiments described in paper **VII** and **VIII**, both hard and soft X-rays were used.

A depth profiling of films of spiro-OMeTAD, DEH and P3HT mixed with Li-TFSI can be seen in figure 5.16. The high binding energy peak at 293 eV seen in spectra of spiro-OMeTAD and DEH corresponds in both cases to the carbon atoms in the TFSI ion. In all cases the feature centered around 285 eV stems from the hole conductor. All peaks at 285 eV are set to the same hight which makes possible a direct comparison between the amounts of Li-TFSI compared to the hole conductor. It is very convenient to be able to measure the contribution from both molecules in the same spectrum. In general, when using synchrotron radiation, the light intensity changes with time and properties that are depending on peak intensity (*e.g.* the amount of a specific element) can be difficult to study. However, when comparing figure 5.16(a) and 5.16(b), it can be seen that for spiro-OMeTAD the contribution from TFSI increases when using lower photon energy, while for DEH the contribution from TFSI is similar for all photon energies. For DEH this means that the Li-salt is more evenly mixed in the molecular film. For spiro-OMeTAD on the other hand, there is a higher concentration of TFSI ions on the molecule/vacuum interface than in the bulk of the sample. Figure 5.17 describes how this depth distribution is affecting the dye-sensitized solar cell, where a very high concentration of Li-TFSI is found at the hole conductor/electrode interface. For P3HT in figure 5.16(c), no sign of the TFSI ion can be seen independent on the photon energy. The presence of Li-TFSI is however still visible through the core level shift in figure 5.13(c). This implies that the Li-TFSI is hidden in the bulk of the sample, under the top P3HT layers.

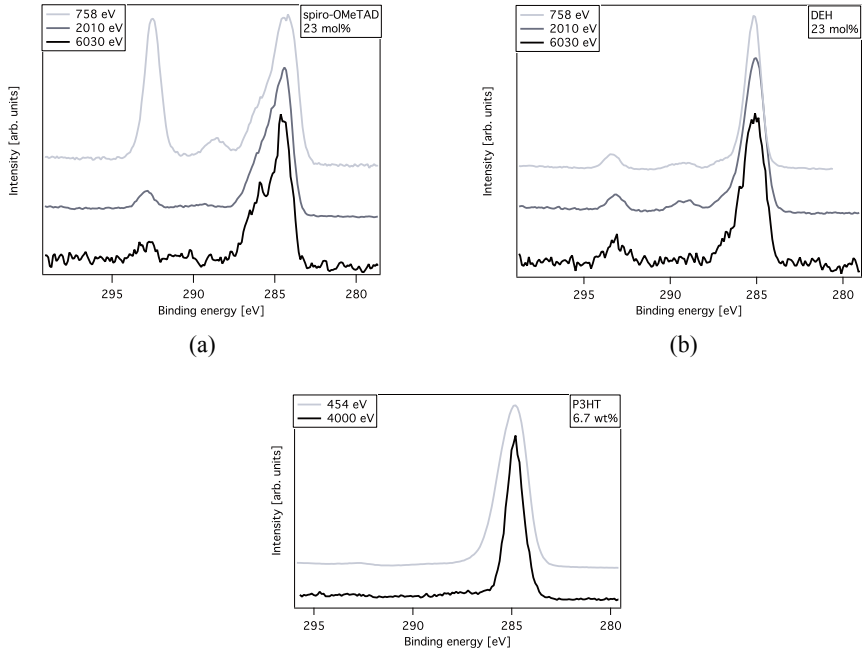

Figure 5.16. The C 1s level of spiro-OMeTAD (a) DEH (b) and P3HT (c) with a high concentration of Li-TFSI measured with different photon energies.

For both spiro-OMeTAD and DEH the intensity of the peak corresponding to the carbon atoms in TFSI ions compared to the hole conductor is larger than what is expected from the preparation concentration. For a preparation concentration of 30 mol% the ratio between the signals from the carbon in the TFSI ion and the hole conductor would be 1% for spiro-OMeTAD and 2.5% for DEH. The actual ratios seen in figure 5.16 is, for a photon energy of 6030 eV, 10% for spiro-OMeTAD and 17% for DEH.

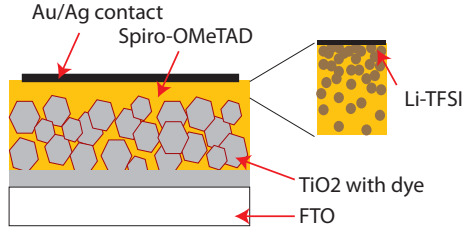

Figure 5.17. The depth distribution of Li-TFSI in a dye-sensitized solar cell with spiro-OMeTAD as hole transporting material.

5.5 Mesoporous TiO_2

Titanumdioxide is a material with many applications as it is cheap, nontoxic and stable and can be found in *e.g.* toothpaste, white paint, sunscreen and in photovoltaic applications. TiO_2 can be found in three different phases: rutile, anatase and brookite. Anatase has the lowest surface energy of the three phases and small particles of TiO_2 therefore have this phase [103]. The most exposed surfaces of anatase are the low index surfaces (101), (001) and (100), where the (101) surface is the most stable [104]. Single crystals of TiO_2 anatase (101) are therefore used as a model surface for nanoparticles in studies of dye adsorption and bonding geometry [105].

A particular property of importance for the function of a mesoscopic oxide structure is the amount of surface defects or vacances. The titanium atoms in TiO_2 has the oxidation number four, Ti^{4+}, while the oxygen atoms have minus two, O^{2-}. Surface defects such as oxygen vacancies can lower the oxidation number of Ti (mainly giving Ti^{3+}). Less positive oxidation numbers generally shifts the level in a photoelectron spectra towards lower binding energy. Oxygen vacancies can therefore be seen as a shoulder on the low binding energy side of Ti core levels or as a state in the bandgap [106].

Nanoparticles of TiO_2 can have a small amount of vacancies giving occupied states in the bandgap that reaches the Fermi level. These bandgap states can be removed by surface treatments using $LiClO_4$ [107] or by adsorption of dye molecules [76]. The bandgap states can also be removed when depositing a metal sulfide on the mesoporous surface as described in paper **III**, see figure 5.18(a). Covering the surface with a perovskite does not, on the other hand, remove the bandgap states as can be seen in figure 5.18(b) (paper **IV**).

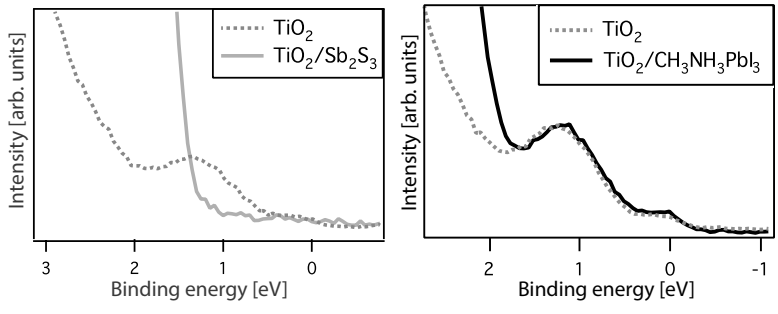

Figure 5.18. The bandgap region measured with a photon energy of 150 eV for TiO_2, TiO_2/sulfide (a) and TiO_2/perovskite (b) interfaces. A low photon energy is useful when studying the weak bandgap states due to a higher photoionization cross section at low binding energies.

5.6 Conducting glass

All mesoscopic solar cells require a transparent, conducting front electrode that also should serve as a substrate for the mesoporous film. Glass with a transparent conducting film fulfill all these requirements and can serve as an important component in practical solar energy devices. Noble metals are good conductors, and a really thin film (a few nm) of, for example, Ag is transparent. It is however difficult to deposit a homogeneous film of a noble metal of such thickness directly on a glass substrate. Therefore, the noble metal layer is placed in a stack of thin films of other metals and metal oxides. One example is stacks of ZnO/Ti/Ag where the metallic Ti acts as an adhesion enhancer between the oxide and the noble metal [108]. The interface between ZnO and Ti is highly reactive and is therefore interesting to study, even without a noble metal, and is the topic of paper **IX**. The buried interfaces in ZnO/Ti and ZnO/Ti/ZnO stacks are best studied with HAXPES.

The oxidation state of Ti and Zn was followed during annealing of sputter deposited ZnO/Ti and ZnO/Ti/ZnO films and the Ti 2p core level can be found in figure 5.19. To protect the surface from oxidation, a capping layer of Mo was deposited on top of both samples. At room temperature the Ti signal in the ZnO/Ti sample showed metallic behaviour. In the ZnO/Ti/ZnO sample the Ti 2p shows several features originating from both metallic and oxidized Ti. From measurements of Zn LMM Auger it could also be seen that at room temperature there were metallic zinc at the interface, indicating a reduction of ZnO during deposition of Ti. Figure 5.20 illustrates to the left the sample geometry at room temperature.

During annealing of the samples in steps up to 550° C, the Ti gets more and more oxidized and for the ZnO/Ti/ZnO sample the Ti is completely oxidized at 550° C. For the ZnO/Ti sample there is still a small contribution of metallic Ti after annealing, which is more pronounced with a lower photon energy, indicating that there are metallic Ti at the sample surface. The left part in figure 5.20 describes the samples after annealing. When depositing Ti on ZnO, the Ti stays mainly metallic even though a small oxidation of Ti and reduction of Zn appears at the interface. When depositing ZnO on top of Ti, the reactive Ti is oxidized during deposition. During annealing, the Ti is further oxidized by oxygen diffusion from the bottom ZnO layer. Peak positions and shapes of the O 1s and Zn 2p core levels together with the relative Ti/Zn and Zn/O ratios indicates the formation of a Zn_xTiO_y compound at the higher annealing temperature.

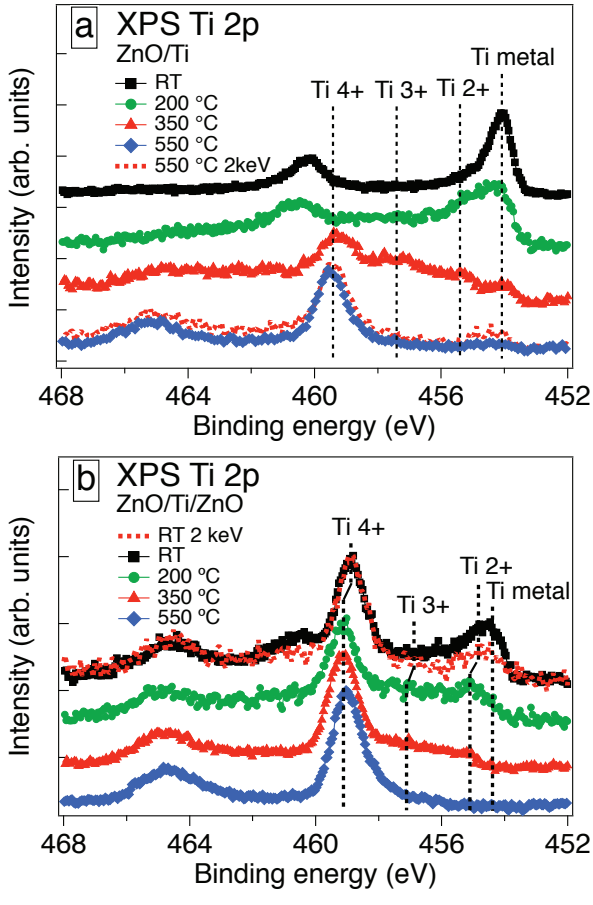

Figure 5.19. The Ti 2p core level in ZnO/Ti (a) and ZnO/Ti/ZnO (b) samples at room temperature and during annealing. The vertical dotted lines indicate the different oxidation states of Ti. A photon energy of 4000 eV was used except for the two spectra marked with 2000 eV.

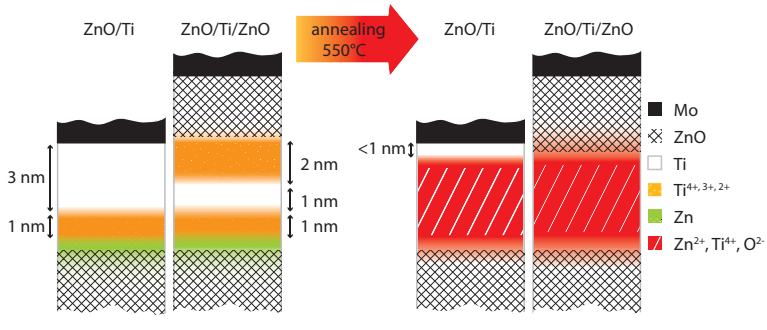

Figure 5.20. Actual sample geometry of ZnO/Ti and ZnO/Ti/ZnO samples at room temperature (left) and after annealing to 500° C (right).

6. Outlook

The work in this thesis shows that photoelectron spectrosocpy can be very useful to study the electronic structure of materials for mesoscopic solar cells. The studies are largely based on developed methodologies using combinations of soft and hard X-ray photoelectron spectroscopy. The main focus has been on the materials themselves as well as the energy level alignment between the different materials in the device. Below I would like to give some examples of emerging complementary X-ray based techniques that allows to study other aspects of the solar cell and the materials involved at an atomic level: angular resolved time-of-flight, ambient pressure photoelectron spectroscopy and X-ray pump-probe techniques.

Many of the investigated systems are very complex, and understanding of their properties would benefit from detailed studies on well defined model systems. For example, model systems of mesoscopic solar cells, such as single crystalline TiO_2 where dye molecules are deposited in vacuum, can be studied to gain detailed information about *e.g.* bonding to the surface [105]. Deeper understanding about the charge transport mechanism in semiconductors can also be obtained by studies of the band structure, which can be achieved by angular resolved photoelectron spectroscopy, a well known technique for inorganics semiconductors. The study of organic single crystalline materials, *e.g.* hole conducting polymers and molecules, is however more challenging due to low conductivity and potential beam damage. Complete band structures of organic single crystals have however been measured with an angular resolved time-of-flight (ARTOF) spectrometer [109]. This type of spectrometer allows measurements over a wide angle and due to a high transmission it can be operated at low photon flux to avoid beam damage. The latter feature can also be used for measuring photoelectron spectra of molecules that are very sensitive to beam damage or are subject to charging.

Moving one step away from studies of model systems in vacuum is ambient pressure photoelectron spectroscopy. This technique allows measurements at relatively high pressures (up to 130 mbar), to study reactions with various gases and to come closer to real conditions [110]. To follow adsorption to a surface or catalytic reactions at a surface are examples of studies that have been performed with ambient pressure photoelectron spectroscopy. For mesoscopic solar cells, this technique opens up for studies of solvation effects from the liquid electrolyte on dye molecules, with the goal of studying a liquid device under operation.

Pump-probe techniques, where one light source excites the system and another light source measures the excited system, allow studies of the fast processes in a solar cell. Especially the excited state of a dye moleucule can be reached with a pump source having a photon energy matching the HOMO-LUMO gap, and the excited dye molecule can then be studied with photoelectron spectroscopy [111]. Short pulsed light sources are required and lasers have typically been used as both pump and probe sources. To probe the full valence region, or core levels, the photon energy of the probe source needs to be higher than what a normal laser can provide, and this can be achieved with a laser driven high-harmonic generation source (HHG), an X-ray free electron laser (XFEL) or a synchrotron. Even though a synchrotron source is pulsed, the number of pulses are high and might need to be lowered to achieve a better time resolution and to match with the pump source. This can be realized by mechanical chopping of the synchrotron beam, or by slicing the beam using a laser [112].

7. Populärvetenskaplig sammanfattning

7.1 Mesoskopiska solceller

Solceller är ett alternativ för en hållbar elproduktion där energin i solljuset omvandlas till elektricitet. I en solcell absorberas solljus varpå elektroner exciteras till högre energinivåer. Elektronen rör sig sedan åt ena hållet och det kvarvarande hålet rör sig åt andra hållet varpå laddningarna separeras.

De första solcellerna tillverkades för över 60 år sedan och sedan dess har mycket forskning bedrivits för att dels göra dem mer effektiva på att omvandla solenergi till elektrisk energi, och dels att göra tillverkningen enklare och mindre energikrävande. De första solcellerna bestod av mycket rent (enkristallint) kisel. En enklare variant ur tillverkningssynpunkt är mesoskopiska solceller, vilket är ett samlingsnamn för olika typer av solceller som använder en nanoporös yta som grund för solcellen[1]. Detta nanoporösa material består av små partiklar av ett halvledarmaterial som bakats ihop till en tvättsvampsliknande struktur. TiO_2 är det vanligaste halvledarmaterialet för detta ändamål, vilket är stabilt och billigt. Problemet med TiO_2 är att det har ett stort bandgap[2] och därför inte absorberar synligt ljus, enbart TiO_2 utgör alltså inte någon bra solcell. Lösningen är att belägga den nanoporösa ytan med ett färgämne, d.v.s. ett material som absorberar synligt ljus. Detta färgämne kan vara en molekyl eller ett halvledarmaterial med ett förhållandevis litet bandgap. Efter att en elektron i färgämnet har exciterats så skickas denna in i den nanoporösa strukturen och leds bort mot en kontakt. I solcellen behövs också något som kan leda hål åt andra hållet (alternativt leda elektroner tillbaka till färgämnet), detta kan vara en flytande elektrolyt eller ett fast, ofta molekylärt, material. I figur 7.1 visas en illustrering av solcellen, i detta fall med en molekyl som färgämne.

De första mesoskopiska solcellerna utvecklades på 1990-talet av en forskargrupp ledd av Michael Grätzel, därför kallas solcellerna ibland för Grätzelceller. Som färgämne användes då en molekyl och för att leda hål användes en flytande elektrolyt [5]. För bara några år sedan började ett organiskt-oorganiskt material med perovskitstruktur att användas som färgämne tillsammans med en fast hålledare. Denna variant blev mycket snabbt den mest effektiva mesoskopiska solcellen och kallas ofta för en perovskitsolcell [14, 15].

För att solcellen ska kunna fungera måste de olika materialen ha energinivåer som förhåller sig på ett visst sätt till varandra, se den högra skissen i figur 7.1.

[1] Mesoskopisk innebär en storleksordning mellan mikroskopisk (från enstaka atomer upp till en storleken av en molekyl) och makroskopisk (då man kan prata om ett fast material).

[2] Ett mellanrum mellan tomma och fyllda energinivåer kallas för ett bandgap och hittas i halvledare och isolatorer, men inte i metaller.

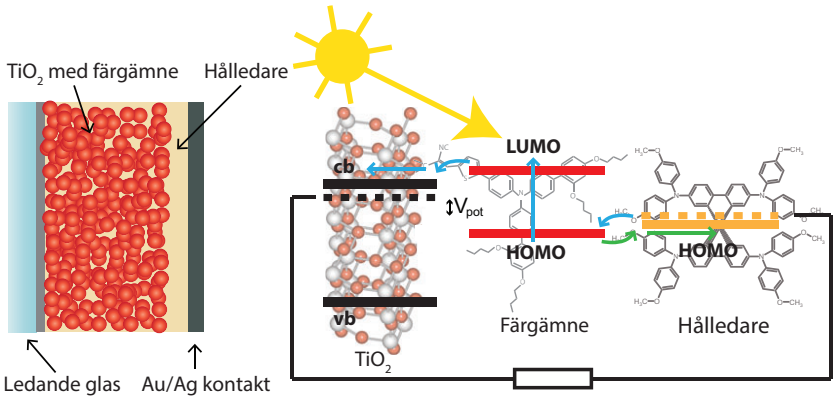

Figure 7.1. En skiss över solcellen (vänster) och de energinivåer som är viktiga för solcellens funktion (höger). Detta exempel visar en färgämnesmolekyl som ljusabsorberare. De blå pilarna visar hur elektronerna rör sig i solcellen och de gröna hur hålen rör sig.

Den lägsta nivån utan elektroner i grundtillståndet i färgämnet (vilket kallas LUMO i en molekyl och ledningsbandet i en halvledare) måste ha en energi som är något högre än ledningsbandet i TiO_2. På samma sätt måste den högsta fyllda nivån (i grundtillståndet) i hålledaren ha en högre energi än motsvarande energinivå i färgämnet (vilket kallas HOMO eller valensbandet). De fyllda energinivåerna går att studera direkt med elektronspektroskopi vilket har varit den huvudsakliga metoden i detta arbete. Mesoskopiska solceller med olika typer av färgämnen: molekyler, halvledare och perovskiter, har undersökts och de olika materialen studeras ensamma eller i kombination. Målet är att förstå, på atomär nivå, hur materialen interagerar med varandra och hur man på olika sätt kan modifiera elektronstrukturen.

7.2 Elektronspektroskopi

Elektronspektroskopin utvecklades under 1960-talet av Kai Siegbahn med medarbetare och är en metod att studera elektronstrukturen i material [38]. Metoden bygger på den fotoelektriska effekten som går ut på att material som blir belyst med röntgenstrålning skickar ut elektroner. Genom att jämföra den kinetiska energin på de utgående fotoelektronerna med energin på röntgenstrålningen kan man bestämma elektronens bindningsenergi i materialet, enligt

$$E_k = h\nu - \Phi - E_b \tag{7.1}$$

där E_k är kinetisk energi, E_b är bindningsenergi, $h\nu$ är energin på röntgenstrålningen och Φ är utträdesarbetet. Tack vare att olika ämnen har mycket specifika energier på de olika energinivåerna kan man ta reda på vilket ämne

det är. Antalet utskickade elektroner mäts som funktion av den kinetiska energin (eller bindningsenergin) och resultatet visas i ett spektrum där varje energinivå ger en linje (som dock har en viss bredd). Energinivåerna påverkas dock av omgivningen vilket gör att olika omgivning ger olika bindningsenergi för samma nivå. Detta syns i ett spektrum som ett kemiskt skift och kan användas för att bestämma hur ämnen reagerar med varandra.

Kärt barn har många namn och akronymerna PES, XPS, ESCA och HAXPES är alla på ett eller annat sätt en förkortning för elektronspektroskopi. Den sista i raden, HAXPES, används om röntgenstrålningen har hög energi (2000 eV och högre), vilket har använts mycket i detta arbete.

Den medelfria väglängden är mycket kort för elektroner, vilket dels innebär att elektronspektroskopiska experiment generellt måste utföras i vakuum. Det innebär också att metoden i allmänhet är ytkänslig eftersom elektroner som kommer från atomer djupare i materialet inte hittar ut ur materialet. Genom att använda röntgenstrålning med högre energi får fotoelektronerna också högre kinetisk energi och då ökar den medelfria väglängden. HAXPES är således en mer bulkkänslig metod och kan användas för att studera material och gränsskikt som ligger under ytan.

7.3 Experimentella resultat

Studier av de energinivåer som är illustrerade i figur 7.1 kan användas för att förstå, och förutse, hur olika material fungerar i en solcell. De energinivåer som är fyllda av elektroner (HOMO för molekyler och valensbandet för halvledare) kan studeras direkt med elektronspektroskopi. Genom att jämföra med mätningar av bandgapet kan även positionen av de tomma nivåerna (LUMO eller ledningsbandet) ritas in ett diagram över energinivåerna i solcellen. I artiklarna **III** och **IV** beskrivs hur detta kan göras för energinivåerna i TiO_2 jämfört med en perovskit eller med metallsulfider och polymerer, se ett exempel i figur 7.2. För sulfiderna kunde energinivådiagrammet användas för att förklara varför två av sulfiderna (Sb_2S_3 och CdS) fungerar som färgämne, medan den tredje inte gör det (Bi_2S_3). Det visade sig att ledningsbanden för Bi_2S_3 och TiO_2 ligger på samma energi, vilket gör att elektronerna i Bi_2S_3 inte har någon drivkraft att ta sig vidare till TiO_2. Studier av djupare liggande energinivåer kan också säga mycket om materialet samt hur det påverkas av olika omgivningar.

För att optimera förhållandet mellan energinivåerna kan det vara av vikt att kunna påverka dessa. Artiklarna **VI**, **VII** och **VIII** beskriver hur detta kan göras för olika hålledande molekylära material. Ett sätt att ändra energinivåförhållandet mellan två olika material, t. ex. en halvledare och en polymer, är att "stoppa in" ett molekylärt material med en dipol [3] mellan de två

[3] En dipol består av ett material, ofta en molekyl, med en bestämd laddningsfördelning som gör att ena sidan av materialet är negativt medan andra sidan är positivt laddat.

andra materialen. Beroende på riktningen på dipolmomentet kan detta skifta energinivåerna i polymeren uppåt eller neråt i förhållande till halvledaren.

Energinivåerna i ett halvledande material (vilket kan vara ett molekylärt material) kan också ändras genom att materialet dopas. Dopning innebär att elektroner tillförs, eller tas bort, varpå ledningsförmågan ökar. I artikel **VIII** studeras hur dopningen kan varieras med olika dopämnen. Artikel **VII** och **VIII** beskriver också hur ett material som inte förväntas fungera som ett dopämne (ett Li-salt) faktiskt ändå påverkar det hålledande materialet på motsvarande sätt.

För molekyler som används som färgämne kan det vara av vikt att molekylen sitter fast på ett visst sätt på ytan av det nanoporösa materialet, för att elektroner lätt ska kunna förflyttas från färgämnet in i den nanoporösa halvledaren. Att tillföra vatten i processen då färgämnet fäster på den nanoporösa ytan har visat sig ändra något hur molekylen sitter, vilket beskrivs i artiklarna **I** och **II**. I en solcell där det nanoporösa materialet bestod av ZnO visade sig också vatten kunna förbättra solcellen, genom att förhindra att molekyler klumpade ihop sig.

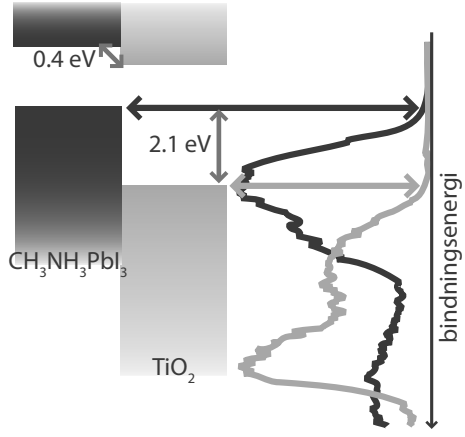

Figure 7.2. Energinivådiagram för ett gränsskikt mellan TiO_2 och perovskiten $CH_3NH_3PbI_3$ (vänster) samt de experimentellt uppmätta valensbanden för TiO_2 och $CH_3NH_3PbI_3$ på TiO_2 (höger). Ledningsbanden för materialen har ritats in i diagrammet med hjälp av optiskt mätta bandgap.

Acknowledgements

I have had the great pleasure to partly be at two departments and to have as many as four supervisors: Håkan, Hans, Anders and Erik. Even though it sometimes took some time to find you all, it was worth it! You have taught me so much about photoelectron spectroscopy, solar cells, and how to study solar cells with photoelectron spectroscopy.

Special thanks to Håkan for always being encouraging and making me want to strive higher.

Erik, thanks for all the time spent in explaining whatever I needed to understand at the moment. Finally you became the supervisor you always were.

Thanks to all recent and former PhD students and post-docs in our solar-cell+PES group with whom I have shared endless hours at different synchrotrons: Susanna, Johan, Stefan, Maria, Bertrand and Sareh. You made it fun!

I have had the opportunity to work with a lot of people in various projects and would like to thank all of you: the Saint-Gobain people Sergey, Elin, Ekaterina, Jean-Yvon, Charlie and Ronny; Davide, Anders, Lars Erik, Andreas S and Mari for teaching me surface science; Mihaela for making the measurements at BESSY fun and easy; Ute, Flannan and Saif for a nice stay in London; Michael and Naresh for interesting calculations; Sara for good collaboration in the course lab; Jill for a fun time at Bessy; all the solar cell people including Kristofer, Martin, Dongqin, Byong-wook, Majid, Maria Q, Tannia, Hanna, Sandra and Gerrit for good work together.

My gratitude goes of course also to the rest of my colleagues at Molecular and Condensed Matter Physics, for company and nice discussions in the coffee room (sometimes during Tisdagsfika): Ieva, Nina, Josephina, Joachim, Olof, Victor, Torsten, Melanie, Richard, Nils, Madelene, Johan S, Svante, Nils, Rein, Olle, Ruben and all the rest of you! So many have crossed my path during the years and I know that the previous list is not complete, but you are not forgotten.

I would also like to thank all my friends outside work, in Uppsala, Paris and Kumla/Örebro: you know who you are!

Min familj, tack för att ni är ni och för att det är så roligt att vara med er!

Andreas, I thank you for always making me laugh and for always being there for me. Love you.

References

[1] D. Elliot. *Renewables. A review of sustainable energy supply options*. IOP Publishing (2013).

[2] M. Grätzel. Photoelectrochemical cells. *Nature*, **414**, 338–344 (2001).

[3] A. M. Green. *Solar cells, Operating Principles, Technology and System Applications*. University of New South Wales, Australia (1992).

[4] S. Schorr, R. Mainz, H. Mönig, I. Lauermann, and M. Bär. The complex material properties of chalcopyrite and kesterite thin-film solar cell absorbers tackled by synchrotron-based analytics. *Prog. Photovoltaics*, **20**, 557–567 (2012).

[5] B. O'Regan and M. Grätzel. A low-cost, high-efficient solar cell based on dye-sensitized colloidal TiO_2 films. *Nature*, **353**, 737–740 (1991).

[6] K. Kalyanasundaram. Photophysics, photochemistry and solar energy conversion with tris(bipyridyl)ruthenium(II) and its analogues. *Coord. Chem. Rev.*, **46**, 159–244 (1982).

[7] A. Hagfeldt, G. Boschloo, L. Sun, L. Kloo, and H. Pettersson. Dye-sensitized solar cells. *Chem. Rev.*, **110**, 6595–6663 (2010).

[8] H. J. Snaith. Perovskites: The Emergence of a New Era for Low-Cost, High-Efficiency Solar Cells. *J. Phys. Chem. Lett.*, **4**, 3623–3630 (2013).

[9] B. O'Regan and D. T. Schwartz. Efficient dye-sensitized charge separation in a wide-band-gap p-n heterojunction. *J. Appl. Phys.*, **80**, 4749–4754 (1996).

[10] U. Bach, D. Lupo, P. Compte, J. E. Moser, F. Weissörtel, J. Salbeck, H. Spreitzer, and M. Grätzel. Solid-state dye-sensitized mesoporous TiO_2 solar cells with high photon-to-electron conversion efficiencies. *Nature*, **395**, 583–585 (1998).

[11] H. J. Rhee, C.-C. Chung, and E. W.-G. Diau. A perspective of mesoscopic solar cells based on metal chalcogenide quantum dots and organometal-halide perovskites. *NPG Asia Mater.*, **5** (2013). doi: 10.1038/am.2013.53.

[12] F. T. F. O'Mahony, T. Lutz, N. Guijarro, R. Gomez, and S. A. Haque. Electron and hole transfer at metal oxide/Sb2S3/spiro-OMeTAD heterojunctions. *Energy Environ. Sci.*, **5**, 9760–9764 (2012).

[13] F. T. F. O'Mahony, U. B. Cappel, N. Tokmoldin, T. Lutz, R. Lindblad, H. Rensmo, and S. A. Haque. Low-Temperature Solution Processing of Mesoporous Metal-Sulfide Semiconductors as Light-Harvesting Photoanodes. *Angew. Chem. Int. Edit.*, **52**, 12047–12051 (2013).

[14] C. Grätzel and S. M. Zakeeruddin. Recent trends in mesoscopic solar cells based on molecular and nanopigment light harvesters. *Mater. Today*, **16**, 11–18 (2013).

[15] N.-G. Park. Organometal Perovskite Light Absorbers Toward a 20% Efficiency Low-Cost Solid-State Mesoscopic Solar Cell. *J. Phys. Chem. Lett.*, **4**, 2423–2429 (2013).

[16] I. Chung, B. Lee, J. He, R. P. H. Chang, and M. G. Kanatzidis. All-solid-state dye-sensitized solar cells with high efficiency. *Nature*, **485**, 486–U94 (2012).

[17] L. Etgar, P. Gao, Z. Xue, Q. Peng, A. K. Chandiran, B. Liu, M. K. Nazeeruddin, and M. Grætzel. Mesoscopic CH3NH3PbI3/TiO2 Heterojunction Solar Cells. *J. Am. Chem. Soc.*, **134**, 17396–17399 (2012).

[18] M. M. Lee, J. Teuscher, T. Miyasaka, T. N. Murakami, and H. J. Snaith. Efficient Hybrid Solar Cells Based on Meso-Superstructured Organometal Halide Perovskites. *Science*, **338**, 643–647 (2012).

[19] M. Liu, M. B. Johnston, and H. J. Snaith. Efficient planar heterojunction perovskite solar cells by vapour deposition. *Nature*, **501**, 395+ (2013).

[20] A. Yella, H-W. Lee, H. N. Tsao, C. Yi, A. K. Chandiran, MD. K. Nazeeruddin, E. W-G. Diau, C-Y. Yeh, S. M. Zakeeruddin, and M. Grätzel. Porphyrin-Sensitized Solar Cells with Cobalt (II/III)-Based Redox Electrolyte Exceed 12 Percent Efficiency. *Science*, **334**, 629–634 (2011).

[21] J. Burschka, A. Dualeh, F. Kessler, E. Baranoff, N.-L. Cevey-Ha, C. Yi, M. K. Nazeeruddin, and M. Grätzel. Tris(2-(1H-pyrazol-1-yl)pyridine)cobalt(III) as p-Type Dopant for Organic Semiconductors and Its Application in Highly Efficient Solid-State Dye-Sensitized Solar Cells. *J. Am. Chem. Soc.*, **133**, 18042–18045 (2011).

[22] C. Kittel. *Introduction to Solid State Physics*. Wiley, seventh edition (1996).

[23] Friedman Atkins. *Molecular Quantum Mechanics*. Oxford University Press, 3rd edition (2001).

[24] J. J. Sakurai. *Modern Quantum Mechanics*. Addison-Wesley Pub., USA, revised edition (1994).

[25] K. Waltzer, B. Maenning, M. Pfeiffer, and K. Leo. Highly Efficient Organic Devices Based on Electrically Doped Transport Layers. *Chem. Rev.*, **107**, 1233–1271 (2007).

[26] H. Ishii, K. Sugiyama, E. Ito, and K. Seki. Energy level alignment and interfacial electronic structures at organic/metal and organic/organic interfaces. *Adv. Mater.*, **11**, 605–625 (1999).

[27] E. M. J. Johansson, M. Odelius, P. G. Karlsson, H. Siegbahn, A. Sandell, and H. Rensmo. Interface electronic states and molecular structure of a triarylamine based hole conductor on rutile TiO_2(110). *J. Chem. Phys.*, **128**, 184709 (2008).

[28] S. Braun, W. R. Salaneck, and M. Fahlman. Energy-Level Alignment at Organic/Metal and Organic/Organic Interfaces. *Adv. Mater.*, **21**, 1450–1472 (2009).

[29] T. Mayer, C. Hein, E. Mankel, W. Jaegermann, M. M. Müller, and H.-J. Kleebe. Fermi level positioning in organic semiconductor phase mixed composites: The internal interface charge transfer doping model. *Org. Electron.*, **13**, 1356–1364 (2012).

[30] J. B. Hudson. *Surface Science, an introduction*. John Wiley and Sons (1992).

[31] S. M. Sze. *Physics of Semiconductor Devices*. Wiley, 2nd edition (1981).

[32] D. T. Clark and W. J. Feast. *Polymer Surfaces*. John Wiley and Sons (1978).

[33] L. Lindell, D. Cakir, G. Brocks, M. Fahlman, and S. Braun. Role of intrinsic molecular dipole in energy level alignment at organic interfaces. *Appl. Phys. Lett.*, **102**223301 (2013).

[34] A. Hagfeldt and M. Grätzel. Light-Induced Redox Reactions in Nanocrystalline Systems. *Chem. Rev.*, **95**, 49–68 (1995).

[35] D. F. Watson and G. J. Meyer. Cation effects in nanocrystalline solar cells. *Coord. Chem. Rev.*, **248**, 1391–1406 (2004).

[36] H. Hertz. Ueber einen Einfluss des ultravioletten Lichtes auf die electrische Entladung. *Annalen der Physik*, **267**, 983–1000 (1887).

[37] A Einstein. Generation and conversion of light with regard to a heuristic point of view. *Annalen der Physik*, **17**, 132–148 (1905).

[38] K. Siegbahn, C. Nordling, A. Fahlman, R. Nordberg, K. Hamrin, J. Hedman, G. Johansson, T. Bergmark, S.-E. Karlsson, I. Lindgren, and B. Lindberg. *ESCA Atomic, Molecular and Solid State Structure Studied by means of Electron Spectroscopy*. Almquist and Wiksells, Uppsala (1967).

[39] A. Lindblad. *A Treatise on the Geometric and Electronic Structure of Clusters: Investigated by Synchrotron Radiation Based Electron Spectroscopies*. PhD thesis, Uppsala University (2008).

[40] J. Végh. The Shirley background revised. *J. Electron. Spectrosc.*, **151**, 159–164 (2006).

[41] S. Doniach and M. Šunjić. Many-electron singularity in X-ray photoemission and X-ray line spectra from metals. *J. Phys. C*, **3**, 285 (1970).

[42] S. Hüfner. *Photoelectron Spectroscopy*. Springer, second edition (1996).

[43] D. Coster and R. De L. Kronig. New type of auger effect and its influence on the x-ray spectrum. *Physica*, **2**, 13–24 (1935).

[44] R. J. Waltman, J. Pacansky, and C. W. Bates. X-ray photoelectron spectroscopic studies on organic photoconductors: evaluation of atomic charges on chlorodiane blue and p-(diethylamino)benzaldehyde diphenylhydrazone. *Chem. Mater.*, **5**, 1799–1804 (1993).

[45] J.F. Moulder, W.F. Stickle, P.E. Sobol, and K.D. Bomben. *Handbok of X-ray Photoelectron Spectroscopy*. Physical Electronics (1995).

[46] J. J. Yeh and I. Lindau. Atomic subshell photoionization cross sections and assymetry parameters: 1<Z<103. *Atomic data and Nuclear data tables*, **32**, 1–155 (1985).

[47] R. Knut, R. Lindblad, M. Gorgoi, H. Rensmo, and O. Karis. High energy photoelectron spectroscopy in basic and applied science: Bulk and interface electronic structure. *J. Electron. Spectrosc.*, **190, Part B**, 278–288 (2013).

[48] O.A. Baschenko and V.I. Nefedov. Relative intensities in x-ray photoelectron spectra: Part IV. The effect of elastic scattering in a solid on the free path of electrons and their angular distribution. *J. Electron. Spectrosc.*, **17**, 405–420 (1979).

[49] M. P. Seah and W. A. Dench. Quantitative electron spectroscopy of surfaces: A standard data base for electron inelastic mean free paths in solids. *Surf. Interf. Anal.*, **1**, 2–11 (1979).

[50] J. Soderstrom, N. Mårtensson, O. Travnikova, M. Patanen, C. Miron, L. J. Sæthre, K. J. Børve, J. J. Rehr, J. J. Kas, F. D. Vila, T. D. Thomas, and S. Svensson. Nonstoichiometric Intensities in Core Photoelectron Spectroscopy. *Phys. Rev. Lett.*, **108** (2012).

[51] E. M. J. Johansson, R. Lindblad, H. Siegbahn, A. Hagfeldt, and H. Rensmo. Atomic and electronic structures of interfaces in dye-sensitized nanostructured solar cells. *ChemPhysChem.* (2014). doi: 10.1002/cphc.201301074.

[52] W. Drube. Photoelectron spectroscopy with hard X-rays. *Nucl. Instrum. Meth. A*, **547**, 87–97 (2005).

[53] M. Gorgoi, S. Svensson, F. Schäfers, G. Öhrwall, M. Mertin, P. Bressler, O. Karis, H. Siegbahn, A. Sandell, H. Rensmo, W. Doherty, C. Jung, W. Braun, and W. Eberhardt. The high kinetic energy photoelectron spectroscopy facility at BESSY progress and first results. *Nucl. Instrum. Meth. A.*, **601**, 48–53 (2009).

[54] W. Kohn. Nobel Lecture: Electronic structure of matter-wave functions and density functionals. *Rev. Mod. Phys.*, **71**, 1253–1266 (1999).

[55] P. Hohenberg and W. Kohn. Inhomogeneous Electron Gas. *Phys. Rev.*, **136**, B864–B871 (1964).

[56] W. Kohn and L. J. Sham. Self-Consistent Equations Including Exchange and Correlation Effects. *Phys. Rev.*, **140**, A1133–A1138 (1965).

[57] F. R. Elder, A. M. Gurewitsch, R. V. Langmuir, and H. C. Pollock. Radiation from Electrons in a Synchrotron. *Phys. Rev.*, **71**, 829–830 (1947).

[58] A. Lindblad, S. Svensson, and K. Tiedtke. *A compendium on beam transport and beam diagnostic methods for Free Electron Lasers*. Deutshes Electronen-Synchrotron DESY (2011).

[59] H. Motz. Applications of the Radiation from Fast Electron Beams. *J. Appl. Phys.*, **22**, 527–535 (1951).

[60] M. G. White, R. A. Rosenberg, G. Gabor, E. D. Poliakoff, G. Thornton, S. H. Southworth, and D. A. Shirley. Time-of-flight photoelectron spectroscopy of gases using synchrotron radiation. *Rev. Sci. Instrum.*, **50**, 1268–1273 (1979).

[61] F. Schaefers, M. Mertin, and M. Gorgoi. KMC-1: A high resolution and high flux soft x-ray beamline at BESSY. *Rev. Sci. Instrum.*, **78**, 123102 (2007).

[62] M. Bassler, J. O. Forsell, O. Björneholm, R. Feifel, M. Jurvansuu, S. Aksela, S. Sundin, S. L. Sorensen, R. Nyholm, A. Ausmees, and S. Svensson. Soft X-ray undulator beam line I411 at MAX-II for gases, liquids and solid samples. *J. Electron. Spectrosc.*, **101-103**, 953 (1999).

[63] U. Bach, Y. Tachibana, J-E. Moser, S. A. Haque, J. R. Durrant, M. Grätzel, and D. R. Klug. Charge Separation in Solid-State Dye-Sensitized Heterojunction Solar Cells. *J. Am. Chem. Soc.*, **121**, 7445–7446 (1999).

[64] E. Edri, S. Kirmayer, D. Cahen, and G. Hodes. High Open-Circuit Voltage Solar Cells Based on Organic-Inorganic Lead Bromide Perovskite. *J. Phys. Chem. Lett.*, **4**, 897–902 (2013).

[65] Y.-L. Lee and Y.-S. Lo. Highly Efficient Quantum-Dot-Sensitized Solar Cell Based on Co-Sensitization of CdS/CdSe. *Adv. Func. Mater.*, **19**, 604–609 (2009).

[66] P. Umari, L. Giacomazzi, F. De Angelis, M. Pastore, and S. Baroni. Energy-level alignment in organic dye-sensitized TiO2; from GW calculations. *J. Chem. Phys*, **139**, 014709 (2013).

[67] B. Wenger, M. Grätzel, and J.-E. Moser. Rationale for Kinetic Heterogeneity of Ultrafast Light-Induced Electron Transfer from Ru(II) Complex Sensitizers to Nanocrystalline TiO2. *J. Am. Chem. Soc.*, **127**, 12150–12151 (2005).

[68] G. Boschloo and A. Hagfeldt. Photoinduced absorption spectroscopy of dye-sensitized nanostructured TiO2. *Chem. Phys. Lett.*, **370**, 381–386 (2003).

[69] G. Boschloo and A. Hagfeldt. Activation energy and electron transport in dye-sensitized TiO2 solar cells. *J. Phys. Chem. B*, **109**, 12093–12098 (2005).

[70] I-K. Ding, N. Tétreault, J. Brillet, B. E. Hardin, E. H. Smith, S. J. Rosenthal, F. Sauvage, M. Grätzel, and M. D. McGehee. Pore-Filling of Spiro-OMeTAD in Solid-State Dye Sensitized Solar Cells: Quantification, Mechanism, and Consequences for Device Performance. *Adv. Func. Mater.*, **19**, 2431–2436 (2009).

[71] U. B. Cappel, E. A. Gibson, A. Hagfeldt, and G. Boschloo. Dye Regeneration by Spiro-MeOTAD in Solid State Dye-Sensitized Solar Cells Studied by Photoinduced Absorption Spectroscopy and Spectroelectrochemistry. *J. Phys. Chem. C*, **113**, 6275–6281 (2009).

[72] L. Yang, U. B. Cappel, E. L. Unger, M. Karlsson, K. M. Karlsson, E. Gabrielsson, L. Sun, G. Boschloo, A. Hagfeldt, and E. M. J. Johansson.

Comparing spiro-OMeTAD and P3HT hole conductors in efficient solid state dye-sensitized solar cells. *Phys. Chem. Chem. Phys.*, **14**, 779–789 (2012).

[73] K. Fredin, E. M. J. Johansson, M. Hahlin, R. Schölin, S. Plogmaker, E. Gabrielsson, L. Sun, and H. Rensmo. Solid state dye-sensitized solar cells prepared by infiltrating a molten hole conductor into a mesoporous film at a temperature below 150 degrees C. *Synthetic Met.*, **161**, 2280–2283 (2011).

[74] S.-J. Moon, J.-H. Yum, R. Humphry-Baker, K. M. Karlsson, D. P. Hagberg, T. Marinado, A. Hagfeldt, L. Sun, M. Grätzel, and M. K. Nazeeruddin. Highly Efficient Organic Sensitizers for Solid-State Dye-Sensitized Solar Cells. *J. Phys. Chem. C*, **113**, 16816–16820 (2009).

[75] L. Schmidt-Mende, U. Bach, R. Humphry-Baker, T. Horiuchi, H. Miura, S. Ito, S. Uchida, and M. Grätzel. Organic Dye for Highly Efficient Solid-State Dye-Sensitized Solar Cells. *Adv. Mater.*, **17**, 813–815 (2005).

[76] U. B. Cappel, A. L. Smeigh, S. Plogmaker, E. M. J. Johansson, H. Rensmo, L. Hammarström, A. Hagfeldt, and G. Boschloo. Characterization of the Interface Properties and Processes in Solid State Dye-Sensitized Solar Cells Employing a Perylene Sensitizer. *J. Phys. Chem. C*, **115**, 4345–4358 (2011).

[77] T. Marinado, M. Hahlin, X. Jiang, M. Quintana, E. M. J. Johansson, E. Gabrielsson, S. Plogmaker, D. P. Hagberg, G. Boschloo, S. M. Zakeeruddin, M. Grätzel, H. Siegbahn, L. Sun, A. Hagfeldt, and H. Rensmo. Surface Molecular Quantification and Photoelectrochemical Characterization of Mixed Organic Dye and Coadsorbent Layers on TiO(2) for Dye-Sensitized Solar Cells. *J. Phys. Chem. C*, **114**, 11903–11910 (2010).

[78] G. Boschloo and A. Hagfeldt. Characteristics of the Iodide/Triiodide Redox Mediator in Dye-Sensitized Solar Cells. *Accounts Chem. Res.*, **42**, 1819–1826 (2009).

[79] S. M. Feldt, E. A. Gibson, E. Gabrielsson, L. Sun, G. Boschloo, and A. Hagfeldt. Design of Organic Dyes and Cobalt Polypyridine Redox Mediators for High-Efficiency Dye-Sensitized Solar Cells. *J. Am. Chem. Soc.*, **132**, 16714–16724 (2010).

[80] K. Westermark, H. Rensmo, H. Siegbahn, K. Keis, A. Hagfeldt, L. Ojamäe, and P. Persson. PES Studies of $RU(dcbpyH_2)_2(NCS)_2$ Adsorption on Nanostructured ZnO for Solar Cell Applications. *J. Phys. Chem. B*, **106**, 10102–10107 (2002).

[81] E. M. J. Johansson, M. Hedlund, H. Siegbahn, and H. Rensmo. Electronic and Molecular Surface Structure of $Ru(tcterpy)(NCS)_3$ and $Ru(dcbpy)_2(NCS)_2$ Adsorbed from Solution onto Nanostructured TiO_2: A Photoelectron Spectroscopy Study. *J. Phys. Chem. B*, **109**, 22256–22263 (2005).

[82] G. Hodes. Comparison of Dye- and Semiconductor-Sensitized Porous Nanocrystalline Liquid Junction Solar Cells. *J. Phys. Chem. C*, **112**, 17778–17787 (2008).

[83] I. Lauermann, M. Bär, and C.-H. Fischer. Synchrotron-based spectroscopy for the characterization of surfaces and interfaces in chalcopyrite thin-film solar cells. *Sol. Energ. Mat. Sol. C.*, **95**, 1495–1508 (2011).

[84] H. Lin, C.P. Huang, W. Li, C. Ni, S. Ismat Shah, and Yao-Hsuan Tseng. Size dependency of nanocrystalline TiO2 on its optical property and photocatalytic reactivity exemplified by 2-chlorophenol. *Appl. Catal. B-Environ.*, **68**, 1–11 (2006).

[85] H.-L. Kim, C.-R-Lee, J.-H. Im, K.-B. Lee T., Moehl, A. Marchioro, S.-J. Moon, R. Humphry-Baker, J.-H. Yum, J.-E. Moser, and *et al.* Lead Iodide Perovskite Sensitized All-Solid-State Submicron Thin Film Mesoscopic Solar Cell with Efficiency Exceeding 9%. *Sci. Rep.*, **2**, 591 (2012).

[86] J. H. Noh, S. H. Im, J. H. Heo, T. N. Mandal, and S. I. Seok. Chemical Management for Colorful, Efficient, and Stable Inorganic-Organic Hybrid Nanostructured Solar Cells. *Nano Lett.*, **13**, 1764–1769 (2013).

[87] J. Burschka, N. Pellet, S.-J. Moon, R. Humphry-Baker, P. Gao, M. K. Nazeeruddin, and M. Grætzel. Sequential deposition as a route to high-performance perovskite-sensitized solar cells. *Nature*, **499**, 316–319 (2013).

[88] A. Kojima, K. Teshima, Y. Shirai, and T. Miyasaka. Organometal Halide Perovskites as Visible-Light Sensitizers for Photovoltaic Cells. *J. Am. Chem. Soc.*, **131**, 6050–6051 (2009).

[89] J.-H. Im, C.-R. Lee, J.-W. Lee, S.-W. Park, and N.-G. Park. 6.5% efficient perovskite quantum-dot-sensitized solar cell. *Nanosc.*, **3**, 4088–4093 (2011).

[90] P. Schulz, E. Edri, S. Kirmayer, G. Hodes, D. Cahen, and A. Kahn. Interface energetics in organo-metal halide perovskite-based photovoltaic cells. *Energy Environ. Sci.*, **7**, 1377–1381 (2014).

[91] K.-J. Jiang, K. Manseki, Y.-H. Yu, N. Masaki, K. Suzuki, Y.-I. Song, and S. Yanagida. Photovoltaics Based on Hybridization of Effective Dye-Sensitized Titanium Oxide and Hole-Conductive Polymer P3HT. *Adv. Func. Mater.*, **19**, 2481–2485 (2009).

[92] X. Liu, W. Zhang, S. Uchida, L. Cai, B. Liu, and S. Ramakrishna. An Efficient Organic-Dye-Sensitized Solar Cell with in situ Polymerized Poly(3,4-ethylenedioxythiophene) as a Hole-Transporting Material. *Adv. Mater.*, **22**, E150–E155 (2010).

[93] E. M. J. Johansson, P.G. Karlsson, M. Hedlund, D. Ryan, H. Siegbahn, and H. Rensmo. Photovoltaic and Interfacial Properties of Heterojunctions Containing Dye-Sensitized Dense TiO2 and Tri-arylamine Derivatives. *Chem. Mater.*, **19**, 2071–2078 (2007).

[94] K. Fredin, E. M.J. Johansson, T. Blom, M. Hedlund, S. Plogmaker, H. Siegbahn, K. Leifer, and H. Rensmo. Using a molten organic conducting material to infiltrate a nanoporous semiconductor film and its use in solid-state dye-sensitized solar cells. *Synthetic Met.*, **159**, 166–170 (2009).

[95] J.-H. Yum, P. Chen, M. Grätzel, and M. K. Nazeeruddin. Recent Developments in Solid-State Dye-Sensitized Solar Cells. *ChemSusChem.*, **1**, 699–707 (2008).

[96] B. Enright, G. Redmond, and D. Fitzmaurice. Spectroscopic determination of flatband potentials for polycrystalline TiO2 electrodes in mixed solvent systems. *J. Phys. Chem.*, **98**, 6195–6200 (1994).

[97] J. Krüger, R. Plass, L. Cevey, M. Piccirelli, and M. Grätzel. High efficiency solid-state photovoltaic device due to inhibition of interface charge recombination. *Appl. Phys. Lett.*, **79**, 2085–2087 (2001).

[98] C. Goh, S. R. Scully, and M. D. McGehee. Title. *J. Appl. Phys.*, **101**, 114503 (2007).

[99] H. J. Snaith and M. Grätzel. Enhanced charge mobility in a molecular hole transporter via addition of redox inactive ionic dopant: Implication to dye-sensitized solar cells. *J. Appl. Phys.*, **89**, 262114 (2006).

[100] A. Abate, T. Leijtens, S. Pathak, J. Teuscher, R. Avolio, M. E. Errico, J. Kirkpatrik, J. M. Ball, P. Docampo, I. McPherson, and H. J. Snaith. Lithium salts as "redox active" p-type dopants for organic semiconductors and their impact in solid-state dye-sensitized solar cells. *Phys. Chem. Chem. Phys.*, **15**, 2572–2579 (2013).

[101] J. Burschka, F. Kessler, M. K. Nazeeruddin, and M. Grätzel. Co(III) Complexes as p-Dopants in Solid-State Dye-Sensitized Solar Cells. *Chem. Mater.*, **25**, 2986–2990 (2013).

[102] S. M. Feldt, G. Wang, G. Boschloo, and A. Hagfeldt. Effects of driving forces for recombination and regeneration on the photovoltaic performance of dye-sensitized solar cells using Cobalt Polypyridine redox couples. *J. Phys. Chem. C*, **115**, 21500–21507 (2011).

[103] A. Zaban, S. T. Aruna, S. Tirosh, B. A. Gregg, and Y. Mastai. The Effect of the Preparation Condition of TiO2 Colloids on Their Surface Structures. *J. Phys. Chem. B*, **104**, 4130–4133 (2000).

[104] U. Diebold, N. Ruzycki, G.S. Herman, and A. Selloni. One step towards bridging the materials gap: surface studies of TiO_2 anatase. *Catal. Today*, **85**, 93–100 (2003).

[105] E. M. J. Johansson, S. Plogmaker, L. E. Walle, R. Schölin, A. Borg, A. Sandell, and H. Rensmo. Comparing Surface Binding of the Maleic Anhydride Anchor Group on Single Crystalline Anatase TiO2 (101), (100), and (001) Surfaces. *J. Phys. Chem. C*, **114**, 15015–15020 (2010).

[106] U. Diebold. The surface science of titanium dioxide. *Surf. Sci. Rep.*, **48**, 53–229 (2003).

[107] U. B. Cappel, A. L. Smeigh, S. Plogmaker, E. M. J. Johansson, H. Rensmo, L. Hammarström, A. Hagfeldt, and G. Boschloo. Characterization of the Interface Properties and Processes in Solid State Dye-Sensitized Solar Cells Employing a Perylene Sensitizer. *J. Phys. Chem. C*, **115**, 4345–4358 (2011).

[108] S.Yu Grachev, A. Mehlich, J.-D. Kamminga, E. Barthel, and E. Söndergård. High-throughput optimization of adhesion in multilayers by superlayer gradients. *Thin Solid Films*, **518**, 6052–6054 (2010).

[109] A. Vollmer, R. Ovsyannikov, M. Gorgoi, S. Krause, M. Oehzelt, A. Lindblad, N. Mårtensson, S. Svensson, P. Karlsson, M. Lundvuist, T. Schmeiler, J. Pflaum, and N. Koch. Two dimensional band structure mapping of organic single crystals using the new generation electron energy analyzer {ARTOF}. *J. Electron. Spectrosc.*, **185**, 55–60 (2012).

[110] D. E. Starr, Z. Liu, M. Havecker, A. Knop-Gericke, and H. Bluhm. Investigation of solid/vapor interfaces using ambient pressure X-ray photoelectron spectroscopy. *Chem. Soc. Rev.*, **42**, 5833–5857 (2013).

[111] S. Plogmaker, P. Linusson, J. H. D. Eland, N. Baker, E. M. J. Johansson, H. Rensmo, R. Feifel, and H. Siegbahn. Versatile high-repetition-rate phase-locked chopper system for fast timing experiments in the vacuum ultraviolet and x-ray spectral region. *Rev. Sci. Instrum.*, **83**, 013115 (2012).

[112] S. Yamamoto and I. Matsuda. Time-Resolved Photoelectron Spectroscopies Using Synchrotron Radiation: Past, Present, and Future. *J. Phys. Soc. Japan*, **82**, 021003 (2013).

Acta Universitatis Upsaliensis

Digital Comprehensive Summaries of Uppsala Dissertations from the Faculty of Science and Technology 1135

Editor: The Dean of the Faculty of Science and Technology

A doctoral dissertation from the Faculty of Science and Technology, Uppsala University, is usually a summary of a number of papers. A few copies of the complete dissertation are kept at major Swedish research libraries, while the summary alone is distributed internationally through the series Digital Comprehensive Summaries of Uppsala Dissertations from the Faculty of Science and Technology. (Prior to January, 2005, the series was published under the title "Comprehensive Summaries of Uppsala Dissertations from the Faculty of Science and Technology".)

Distribution: publications.uu.se
urn:nbn:se:uu:diva-221450

ACTA
UNIVERSITATIS
UPSALIENSIS
UPPSALA
2014